EUROPEAN LABORATORY FOR PARTICLE PHYSICS

CERN-PPE/97-015
4 February 1997

QCD studies with e^+e^- annihilation data at 161 GeV

The OPAL Collaboration

Abstract

We have studied hadronic events produced at LEP at a centre-of-mass energy of 161 GeV. We present distributions of event shape variables, jet rates, charged particle momentum spectra and multiplicities. We determine the strong coupling strength to be $\alpha_s(161\ \mathrm{GeV}) = 0.101 \pm 0.005(\mathrm{stat.}) \pm 0.007(\mathrm{syst.})$, the mean charged particle multiplicity to be $\langle n_{\mathrm{ch}} \rangle(161\ \mathrm{GeV}) = 24.46 \pm 0.45(\mathrm{stat.}) \pm 0.44(\mathrm{syst.})$ and the position of the peak in the $\xi_p = \ln(1/x_p)$ distribution to be $\xi_0(161\ \mathrm{GeV}) = 4.00 \pm 0.03(\mathrm{stat.}) \pm 0.02(\mathrm{syst.})$. These results are compared to data taken at lower centre-of-mass energies and to analytic QCD or Monte Carlo predictions. Our measured value of $\alpha_s(161\ \mathrm{GeV})$ is consistent with other measurements of α_s. Within the current statistical and systematic uncertainties, the PYTHIA, HERWIG and ARIADNE QCD Monte Carlo models and analytic calculations are in overall agreement with our measurements. The COJETS QCD Monte Carlo is in general agreement with the data for momentum weighted distributions like Thrust, but predicts a significantly larger charged particle multiplicity than is observed experimentally.

Submitted to Zeitschrift für Physik C

The OPAL Collaboration

K. Ackerstaff[8], G. Alexander[23], J. Allison[16], N. Altekamp[5], K. Ametewee[25],
K.J. Anderson[9], S. Anderson[12], S. Arcelli[2], S. Asai[24], D. Axen[29], G. Azuelos[18,a],
A.H. Ball[17], E. Barberio[8], R.J. Barlow[16], R. Bartoldus[3], J.R. Batley[5], J. Bechtluft[14],
C. Beeston[16], T. Behnke[8], A.N. Bell[1], K.W. Bell[20], G. Bella[23], S. Bentvelsen[8], P. Berlich[10],
S. Bethke[14], O. Biebel[14], A. Biguzzi[5], S.D. Bird[16], V. Blobel[27], I.J. Bloodworth[1],
J.E. Bloomer[1], M. Bobinski[10], P. Bock[11], D. Bonacorsi[2], H.M. Bosch[11], M. Boutemeur[34],
B.T. Bouwens[12], S. Braibant[12], R.M. Brown[20], H.J. Burckhart[8], C. Burgard[8], R. Bürgin[10],
P. Capiluppi[2], R.K. Carnegie[6], A.A. Carter[13], J.R. Carter[5], C.Y. Chang[17],
D.G. Charlton[1,b], D. Chrisman[4], P.E.L. Clarke[15], I. Cohen[23], J.E. Conboy[15], O.C. Cooke[16],
M. Cuffiani[2], S. Dado[22], C. Dallapiccola[17], G.M. Dallavalle[2], S. De Jong[12], L.A. del Pozo[4],
K. Desch[3], M.S. Dixit[7], E. do Couto e Silva[12], M. Doucet[18], E. Duchovni[26], G. Duckeck[34],
I.P. Duerdoth[16], D. Eatough[16], J.E.G. Edwards[16], P.G. Estabrooks[6], H.G. Evans[9],
M. Evans[13], F. Fabbri[2], M. Fanti[2], P. Fath[11], A.A. Faust[30], F. Fiedler[27], M. Fierro[2],
H.M. Fischer[3], R. Folman[26], D.G. Fong[17], M. Foucher[17], A. Fürtjes[8], P. Gagnon[7],
J.W. Gary[4], J. Gascon[18], S.M. Gascon-Shotkin[17], N.I. Geddes[20], C. Geich-Gimbel[3],
T. Geralis[20], G. Giacomelli[2], P. Giacomelli[4], R. Giacomelli[2], V. Gibson[5], W.R. Gibson[13],
D.M. Gingrich[30,a], D. Glenzinski[9], J. Goldberg[22], M.J. Goodrick[5], W. Gorn[4], C. Grandi[2],
E. Gross[26], J. Grunhaus[23], M. Gruwé[8], C. Hajdu[32], G.G. Hanson[12], M. Hansroul[8],
M. Hapke[13], C.K. Hargrove[7], P.A. Hart[9], C. Hartmann[3], M. Hauschild[8], C.M. Hawkes[5],
R. Hawkings[27], R.J. Hemingway[6], M. Herndon[17], G. Herten[10], R.D. Heuer[8],
M.D. Hildreth[8], J.C. Hill[5], S.J. Hillier[1], T. Hilse[10], P.R. Hobson[25], R.J. Homer[1],
A.K. Honma[28,a], D. Horváth[32,c], R. Howard[29], R.E. Hughes-Jones[16], D.E. Hutchcroft[5],
P. Igo-Kemenes[11], D.C. Imrie[25], M.R. Ingram[16], K. Ishii[24], A. Jawahery[17], P.W. Jeffreys[20],
H. Jeremie[18], M. Jimack[1], A. Joly[18], C.R. Jones[5], G. Jones[16], M. Jones[6], R.W.L. Jones[8],
U. Jost[11], P. Jovanovic[1], T.R. Junk[8], D. Karlen[6], K. Kawagoe[24], T. Kawamoto[24],
R.K. Keeler[28], R.G. Kellogg[17], B.W. Kennedy[20], J. Kirk[29], S. Kluth[8], T. Kobayashi[24],
M. Kobel[10], D.S. Koetke[6], T.P. Kokott[3], M. Kolrep[10], S. Komamiya[24], T. Kress[11],
P. Krieger[6], J. von Krogh[11], P. Kyberd[13], G.D. Lafferty[16], R. Lahmann[17], W.P. Lai[19],
D. Lanske[14], J. Lauber[15], S.R. Lautenschlager[31], J.G. Layter[4], D. Lazic[22], A.M. Lee[31],
E. Lefebvre[18], D. Lellouch[26], J. Letts[12], L. Levinson[26], C. Lewis[15], S.L. Lloyd[13],
F.K. Loebinger[16], G.D. Long[28], M.J. Losty[7], J. Ludwig[10], A. Macchiolo[2],
A. Macpherson[30], M. Mannelli[8], S. Marcellini[2], C. Markus[3], A.J. Martin[13], J.P. Martin[18],
G. Martinez[17], T. Mashimo[24], W. Matthews[25], P. Mättig[3], W.J. McDonald[30],
J. McKenna[29], E.A. Mckigney[15], T.J. McMahon[1], A.I. McNab[13], R.A. McPherson[8],
F. Meijers[8], S. Menke[3], F.S. Merritt[9], H. Mes[7], J. Meyer[27], A. Michelini[2], G. Mikenberg[26],
D.J. Miller[15], R. Mir[26], W. Mohr[10], A. Montanari[2], T. Mori[24], M. Morii[24], U. Müller[3],
K. Nagai[26], I. Nakamura[24], H.A. Neal[8], B. Nellen[3], B. Nijjhar[16], R. Nisius[8], S.W. O'Neale[1],
F.G. Oakham[7], F. Odorici[2], H.O. Ogren[12], N.J. Oldershaw[16], T. Omori[24], M.J. Oreglia[9],
S. Orito[24], J. Pálinkás[33,d], G. Pásztor[32], J.R. Pater[16], G.N. Patrick[20], J. Patt[10],
M.J. Pearce[1], S. Petzold[27], P. Pfeifenschneider[14], J.E. Pilcher[9], J. Pinfold[30], D.E. Plane[8],
P. Poffenberger[28], B. Poli[2], A. Posthaus[3], H. Przysiezniak[30], D.L. Rees[1], D. Rigby[1],
S. Robertson[28], S.A. Robins[13], N. Rodning[30], J.M. Roney[28], A. Rooke[15], E. Ros[8],

A.M. Rossi[2], M. Rosvick[28], P. Routenburg[30], Y. Rozen[22], K. Runge[10], O. Runolfsson[8], U. Ruppel[14], D.R. Rust[12], R. Rylko[25], K. Sachs[10], E.K.G. Sarkisyan[23], M. Sasaki[24], C. Sbarra[29], A.D. Schaile[34], O. Schaile[34], F. Scharf[3], P. Scharff-Hansen[8], P. Schenk[34], B. Schmitt[8], S. Schmitt[11], M. Schröder[8], H.C. Schultz-Coulon[10], M. Schulz[8], M. Schumacher[3], P. Schütz[3], W.G. Scott[20], T.G. Shears[16], B.C. Shen[4], C.H. Shepherd-Themistocleous[8], P. Sherwood[15], G.P. Siroli[2], A. Sittler[27], A. Skillman[15], A. Skuja[17], A.M. Smith[8], T.J. Smith[28], G.A. Snow[17], R. Sobie[28], S. Söldner-Rembold[10], R.W. Springer[30], M. Sproston[20], A. Stahl[3], M. Steiert[11], K. Stephens[16], J. Steuerer[27], B. Stockhausen[3], D. Strom[19], P. Szymanski[20], R. Tafirout[18], S.D. Talbot[1], S. Tanaka[24], P. Taras[18], S. Tarem[22], M. Thiergen[10], M.A. Thomson[8], E. von Törne[3], S. Towers[6], I. Trigger[18], T. Tsukamoto[24], E. Tsur[23], A.S. Turcot[9], M.F. Turner-Watson[8], P. Utzat[11], R. Van Kooten[12], M. Verzocchi[10], P. Vikas[18], M. Vincter[28], E.H. Vokurka[16], F. Wäckerle[10], A. Wagner[27], C.P. Ward[5], D.R. Ward[5], J.J. Ward[15], P.M. Watkins[1], A.T. Watson[1], N.K. Watson[1], P.S. Wells[8], N. Wermes[3], J.S. White[28], B. Wilkens[10], G.W. Wilson[27], J.A. Wilson[1], G. Wolf[26], S. Wotton[5], T.R. Wyatt[16], S. Yamashita[24], G. Yekutieli[26], V. Zacek[18], D. Zer-Zion[8]

[1]School of Physics and Space Research, University of Birmingham, Birmingham B15 2TT, UK
[2]Dipartimento di Fisica dell' Università di Bologna and INFN, I-40126 Bologna, Italy
[3]Physikalisches Institut, Universität Bonn, D-53115 Bonn, Germany
[4]Department of Physics, University of California, Riverside CA 92521, USA
[5]Cavendish Laboratory, Cambridge CB3 0HE, UK
[6] Ottawa-Carleton Institute for Physics, Department of Physics, Carleton University, Ottawa, Ontario K1S 5B6, Canada
[7]Centre for Research in Particle Physics, Carleton University, Ottawa, Ontario K1S 5B6, Canada
[8]CERN, European Organisation for Particle Physics, CH-1211 Geneva 23, Switzerland
[9]Enrico Fermi Institute and Department of Physics, University of Chicago, Chicago IL 60637, USA
[10]Fakultät für Physik, Albert Ludwigs Universität, D-79104 Freiburg, Germany
[11]Physikalisches Institut, Universität Heidelberg, D-69120 Heidelberg, Germany
[12]Indiana University, Department of Physics, Swain Hall West 117, Bloomington IN 47405, USA
[13]Queen Mary and Westfield College, University of London, London E1 4NS, UK
[14]Technische Hochschule Aachen, III Physikalisches Institut, Sommerfeldstrasse 26-28, D-52056 Aachen, Germany
[15]University College London, London WC1E 6BT, UK
[16]Department of Physics, Schuster Laboratory, The University, Manchester M13 9PL, UK
[17]Department of Physics, University of Maryland, College Park, MD 20742, USA
[18]Laboratoire de Physique Nucléaire, Université de Montréal, Montréal, Quebec H3C 3J7, Canada
[19]University of Oregon, Department of Physics, Eugene OR 97403, USA
[20]Rutherford Appleton Laboratory, Chilton, Didcot, Oxfordshire OX11 0QX, UK

[22]Department of Physics, Technion-Israel Institute of Technology, Haifa 32000, Israel
[23]Department of Physics and Astronomy, Tel Aviv University, Tel Aviv 69978, Israel
[24]International Centre for Elementary Particle Physics and Department of Physics, University of Tokyo, Tokyo 113, and Kobe University, Kobe 657, Japan
[25]Brunel University, Uxbridge, Middlesex UB8 3PH, UK
[26]Particle Physics Department, Weizmann Institute of Science, Rehovot 76100, Israel
[27]Universität Hamburg/DESY, II Institut für Experimental Physik, Notkestrasse 85, D-22607 Hamburg, Germany
[28]University of Victoria, Department of Physics, P O Box 3055, Victoria BC V8W 3P6, Canada
[29]University of British Columbia, Department of Physics, Vancouver BC V6T 1Z1, Canada
[30]University of Alberta, Department of Physics, Edmonton AB T6G 2J1, Canada
[31]Duke University, Dept of Physics, Durham, NC 27708-0305, USA
[32]Research Institute for Particle and Nuclear Physics, H-1525 Budapest, P O Box 49, Hungary
[33]Institute of Nuclear Research, H-4001 Debrecen, P O Box 51, Hungary
[34]Ludwigs-Maximilians-Universität München, Sektion Physik, Am Coulombwall 1, D-85748 Garching, Germany

[a] and at TRIUMF, Vancouver, Canada V6T 2A3
[b] and Royal Society University Research Fellow
[c] and Institute of Nuclear Research, Debrecen, Hungary
[d] and Department of Experimental Physics, Lajos Kossuth University, Debrecen, Hungary

1 Introduction

The upgrade of LEP to a centre-of-mass (c.m.) energy $\sqrt{s} \approx 161$ GeV provides an opportunity to study QCD at energies in e^+e^- collisions higher than previously published. The general features of hadronic events may be described by event shape distributions and charged particle momentum spectra which are sensitive to the energy and momentum flow of the particles in the events. The particles may also be clustered into jets. The distributions of the event shapes and the jet production rates are characteristic features of the multihadron production process. Predictions for these distributions may be obtained from QCD based Monte Carlo models which include perturbative and non-perturbative effects. In some cases, predictions from analytic QCD calculations are also available. Studies using e^+e^- annihilation data at c.m. energies up to $\sqrt{s} = 130 - 136$ GeV have previously shown that these QCD based models and calculations give a good overall description of the observed data [1–6]. It is an important test of the overall consistency of QCD that data at yet higher c.m. energies should also be well described.

The majority of hadronic events produced at c.m. energies above the Z^0 resonance are "radiative" events in which initial state photon radiation (ISR) reduces the energy of the hadronic system to about M_{Z^0}. The study of hadronic events at the highest possible energies requires an experimental separation between radiative and non-radiative events. At energies above about 161 GeV, W^+W^- production becomes kinematically possible, and the hadronic decays of the W bosons will contribute background to the non-radiative $(Z^0/\gamma)^*$ events.

We present a study of hadronic events recorded by the OPAL detector during the LEP run of July to August 1996 at a c.m. energy of 161 GeV. The same techniques are used as in our previous analysis of e^+e^- annihilation data at energies of 130–136 GeV [1]. Section 2 gives a brief description of the OPAL detector, section 3 explains the samples of data and simulated events used in this paper and section 4 deals with our analysis procedures. Section 5 contains the results of the analyses and section 6 gives a summary and conclusion.

2 The OPAL detector

The OPAL detector operates at the LEP e^+e^- collider at CERN. A detailed description can be found in reference [7]. The analysis presented here relies mainly on the reconstruction of charged particles in the tracking chambers and of energy deposits ("clusters") in the electromagnetic calorimeters.

All tracking systems are located inside a solenoidal magnet which provides a uniform axial magnetic field of 0.435 T along the beam axis[1]. The magnet is surrounded by a lead glass electromagnetic calorimeter and a hadron calorimeter of the sampling type. Outside the hadron calorimeter, the detector is surrounded by a system of muon chambers. There are similar layers of detectors in the endcap regions.

[1]In the OPAL coordinate system the x axis points towards the centre of the LEP ring, the y axis points upwards and the z axis points in the direction of the electron beam. The polar angle θ and the azimuthal angle ϕ are defined with respect to the z- and x-axes, respectively, while r is the distance from the z-axis.

The main tracking detector is the central jet chamber. This device is approximately 4 m long and has an outer radius of about 1.85 m. It has 24 sectors with radial planes of 159 sense wires spaced by 1 cm. The momenta, p_{xy}, of tracks in the x-y plane are measured with a precision parametrised by $\sigma_p/p_{\mathrm{xy}} = \sqrt{(0.02)^2 + (0.0015 \cdot p_{\mathrm{xy}}[\mathrm{GeV}/c])^2}$.

The electromagnetic calorimeters in the barrel and the endcap sections of the detector consist of a total of 11 704 lead glass blocks, with a depth of 24.6 radiation lengths in the barrel and more than 22 radiation lengths in the endcap regions. Each lead glass block subtends approximately 40×40 mrad^2 at the origin.

3 Data and Monte Carlo samples

The data sample used in this analysis corresponds to an integrated luminosity of 10.0 pb^{-1}, collected at a c.m. energy of 161.33 ± 0.05 GeV [8]. Hadronic events are identified using the criteria described in reference [9]. The efficiency for selecting non-radiative hadronic decays is essentially unchanged when compared to lower c.m. energies and is close to 100% [10]. We define as particles both tracks recorded in the tracking chambers, with transverse momentum $p_{\mathrm{xy}} > 150$ MeV$/c$, and clusters recorded in the electromagnetic calorimeter, with a minimum energy of 100 MeV in the barrel and 250 MeV in the endcap sections [1]. We require events to have at least seven accepted tracks and we further require θ_T, the polar angle of the thrust axis found using all accepted tracks and clusters, to lie in the region $|\cos\theta_T| < 0.9$. After these cuts, a total of 1 336 hadronic events are observed.

All Monte Carlo event samples were generated at a c.m. energy of 161.0 GeV. Events with full simulation of the OPAL detector [11] were generated for the process $\mathrm{e^+e^-} \to (\mathrm{Z}^0/\gamma)^* \to \mathrm{q\bar{q}}$ and will be referred to as "$(\mathrm{Z}^0/\gamma)^*$ events". We use a sample of 200 000 (~ 1.4 fb^{-1}) $(\mathrm{Z}^0/\gamma)^*$ events generated using the PYTHIA 5.722 [12] parton shower Monte Carlo with initial and final state photon radiation and fragmentation of the parton final state handled by the routines of JETSET 7.408 [12]. The Monte Carlo parameters have been tuned to OPAL data taken at the Z^0 peak [13] and give a good description of experimental data for $\mathrm{e^+e^-}$ annihilations with c.m. energies from 10 GeV to 136 GeV [1–6]. As an alternative sample, we use 100 000 events generated with the HERWIG 5.8d [14] parton shower Monte Carlo, also tuned to OPAL data [13].

In addition we generated, with full simulation of the OPAL detector, events of the type $\mathrm{e^+e^-} \to 4$ fermions (diagrams without intermediate gluons). These 4-fermion events, in particular those with four quarks in the final state, constitute a background for this analysis. Simulated 4-fermion events with quarks and charged leptonic final states, produced via s-channel or t-channel (where possible) diagrams and including $\mathrm{W^+W^-}$ events, were generated using the grc4f 1.2 Monte Carlo model [15][2]. This generator is interfaced to JETSET 7.4 using the same parameter set for the parton shower, fragmentation and decays as mentioned above for $(\mathrm{Z}^0/\gamma)^*$ events. We employ in total 49 000 (~ 15.5 fb^{-1})

[2]The production cross section for $\mathrm{W^+W^-}$ events is estimated to be 3.44 pb at a c.m. energy of 161.0 GeV and 3.77 pb at 161.33 GeV (assuming a W mass of 80.33 GeV$/c^2$ [16]), using the GENTLE [17] Monte Carlo program. We use this information to correct Monte Carlo estimates of the $\mathrm{W^+W^-}$ production rate for the difference in c.m. energy between the data and Monte Carlo.

4-fermion events. Final states of the type $(Z^0/\gamma)^* e^+e^-$ with one or more electrons produced close to the beam direction, which are not included in the grc4f sample, are added using PYTHIA.

For detailed studies of 4-fermion events arising from W^+W^- production, we use 99 000 ($\sim$ 28.8 fb^{-1}) events from PYTHIA. An alternative sample of 4-fermion events (excluding forward $(Z^0/\gamma)^*$ e^+e^- events) is provided by the EXCALIBUR [18] Monte Carlo program, interfaced to JETSET 7.4 in the same way as grc4f.

In addition to the Monte Carlo event generators discussed above, we use the QCD based event generators ARIADNE 4.08 [19] and COJETS 6.23 [20] in our study. ARIADNE is used to provide a systematic check on the hadronization corrections for our α_s measurement (section 5.3), while both COJETS and ARIADNE are used in addition to PYTHIA and HERWIG to compare to our corrected data distributions. The parameter sets used for ARIADNE and COJETS are documented in [19] and [21]; both models provide a good description of global e^+e^- event properties at $\sqrt{s} = M_{Z^0}$, as do PYTHIA and HERWIG.

4 Data analysis

4.1 Selection of non-radiative events

As in our analysis of 130–136 GeV data, we apply cuts to reject events with energetic initial state radiation and events that are not hadronic decays of a $(Z^0/\gamma)^*$. For Monte Carlo we define non-radiative events using the true effective c.m. energy of the hadronic system, $\sqrt{s'_{\mathrm{true}}}$, determined from Monte Carlo information, by $\sqrt{s} - \sqrt{s'_{\mathrm{true}}} < 1$ GeV.

To reject radiative events, we determine the effective c.m. energy of the observed hadronic system, $\sqrt{s'}$, by either finding isolated neutral clusters in the electromagnetic calorimeter or by performing a kinematic fit to the hadronic system allowing for one unobserved photon close to the beam direction. Events with $\sqrt{s} - \sqrt{s'} < 10$ GeV are selected. This is referred to as the "ISR fit" selection. For systematic studies we use an alternative selection based on measurements of energy and momentum which we denote as the "energy balance" selection. Both of these selections are described in references [1,22]. In Figure 1 we show the $\sqrt{s'}$ distribution for the data and for PYTHIA and grc4f events with full detector simulation. The Monte Carlo events are classified into radiative $(Z^0/\gamma)^*$ events and 4-fermion events.

Based on Monte Carlo studies we find that 7% of the events selected by the ISR fit are 4-fermion events, and 6% are strongly radiative events, with $\sqrt{s} - \sqrt{s'_{\mathrm{true}}} > 10$ GeV. The efficiency of the ISR fit selection to identify non-radiative $(Z^0/\gamma)^*$ events is 93% which gives an overall efficiency for the selection of 82%. The energy balance selection results in an efficiency of 95% and a 4-fermion background of 7%, but a larger (17%) contamination from strongly radiative events. Over 95% of the non-radiative events selected by the ISR fit method are also selected by the energy balance method. Similar estimates of efficiencies and backgrounds are obtained if HERWIG is used instead of PYTHIA.

We select 307 non-radiative events using the ISR fit selection. The background from $e^+e^- \to \tau^+\tau^-$ and two-photon events of the type $\gamma\gamma \to q\bar{q}$ is estimated from Monte Carlo samples to be less than 0.3% and is consequently neglected. We expect to select 21

4-fermion events (i.e. 7%) with the ISR fit selection, according to Monte Carlo studies. The Monte Carlo predicts that about 16 of these 4-fermion events originate from W^+W^- production.

4.2 Correction procedures and treatment of 4-fermion background

Bin-by-bin corrections are applied to the experimental distributions in a two stage process. In the first stage we correct for the presence of background from 4-fermion events. In the second stage, we use a bin-by-bin multiplication procedure to correct the observed distributions for the effects of detector resolution and acceptance as well as for the presence of radiative $(Z^0/\gamma)^*$ events. For the multiplicity measurement presented in section 5.5, we use a matrix correction procedure to account for detector effects and radiative events rather than a bin-by-bin procedure.

Two methods are used to correct for the background from 4-fermion events. The first method, adopted as standard, subtracts the Monte Carlo expectation for the 4-fermion background from the observed distributions. The second method, used as a systematic check, applies a cut designed to reduce the fraction of 4-fermion events coming from W^+W^- production, followed by a subtraction of the remaining background expectation. This remaining background subtraction is smaller than for the standard method, but the procedure introduces a small additional bias in the selected $(Z^0/\gamma)^*$ event sample.

To remove 4-fermion events for the systematic check mentioned in the previous paragraph, we require four jets to be reconstructed in an event, using the Durham jet finder [23]. The invariant mass between pairs of jets, M_W^{fit}, is found by means of a kinematic fit constrained to result in the same mass for both pairs of jets [24]. We reject events with $M_W^{fit} > 72$ GeV/c^2. Applying the ISR fit selection and this cut, we reduce the 4-fermion event background to 3% whereas non-radiative $(Z^0/\gamma)^*$ events are retained with an overall efficiency of about 68%, according to PYTHIA. The effect of this cut on our data sample is consistent with the MC expectation including W^+W^- production (for details see [24]).

For the bin-by-bin correction procedure, each bin of each observable is corrected from the "detector-level" to the "hadron-level" using two samples of Monte Carlo $(Z^0/\gamma)^*$ events generated at $\sqrt{s}$=161.0 GeV. The hadron-level does not include initial state radiation or detector effects and allows all particles with lifetimes shorter than 3×10^{-10} s to decay. The detector-level includes full simulation of the OPAL detector and initial state radiation and contains only those events which pass the same cuts as are applied to the data. The bin-by-bin correction factors are derived from the ratio of the distributions at the hadron-level to those at the detector-level.

4.3 Systematic uncertainties

The experimental systematic uncertainty is estimated by repeating the analysis with information from tracks only or from electromagnetic clusters only. For each measurement, e.g. in a bin of a distribution, the largest of the three differences between the standard result, the one obtained using only tracks and the one obtained using only clusters is used to define this uncertainty.

The homogeneity of the response of the detector in the endcap region was checked by restricting the analysis to the barrel region of the detector, requiring the thrust axis of accepted events to lie within the range $|\cos\theta_T| < 0.7$. The difference relative to the standard analysis is taken to be this uncertainty.

For observables measured using information from charged particles only, we evaluate an additional uncertainty on the track modelling. The largest effect was found by varying the maximum allowed distance of the point of closest approach of a track to the collision point in the r-ϕ plane, d_0. The variation of the observables when d_0 was changed from 2 to 5 cm is taken to be this uncertainty.

Uncertainties arising from the selection of non-radiative events are estimated by repeating the analysis using the energy balance selection. The difference relative to the standard result is taken as the systematic error.

Systematic uncertainties associated with the Monte Carlo description of 4-fermion events are estimated by comparing the results obtained using the ISR fit selection (standard) with those obtained using the ISR fit selection and the additional cut on M_{W}^{fit}. As a check of the simulation of non-$\mathrm{W}^+\mathrm{W}^-$ four fermion events, our standard 4-fermion Monte Carlo generator, grc4f, is replaced by EXCALIBUR. In both cases the difference relative to the standard analysis defines the uncertainty. Effects due to the uncertainties of the $\mathrm{W}^+\mathrm{W}^-$ production cross section are found to be negligible [24].

The difference in the results when we use simulated $(\mathrm{Z}^0/\gamma)^*$ events generated using HERWIG instead of PYTHIA is taken as the uncertainty in the modelling of the $(\mathrm{Z}^0/\gamma)^*$ events.

Due to the relatively small number of selected non-radiative events in this analysis, part of the observed differences when the systematic conditions are varied may be due to statistical fluctuations, especially for those systematic checks in which the composition of the event sample or the set of tracks and/or clusters changes. In order to estimate the statistical components of the systematic terms, we apply the following procedure. A set of 30 independent samples of simulated events, containing on average the same number of events as the data, is passed through the same standard and systematically changed analysis procedures as the data. For each systematic change of the analysis, the variances σ^2 of the differences between the results for this change and the standard results are determined. These variances are compared to the actual differences δ observed in the data when the analysis is changed. We define the systematic error to be $\sigma_{(\mathrm{syst.})} = \sqrt{\delta^2 - \sigma^2}$ $(\delta > \sigma)$ or $\sigma_{(\mathrm{syst.})} = 0$ $(\delta \leq \sigma)$, which reduces the possible overestimation of systematic errors. In order to reduce bin-to-bin fluctuations in the magnitudes of the systematic uncertainties, we average the relative uncertainty over three neighbouring bins.

5 Results

5.1 Event shape observables

We study the event shape observables Thrust (T), Thrust Major and Minor (T_{major} and T_{minor}), Oblateness (O), Sphericity (S), Aplanarity (A), C-parameter (C), Heavy Jet Mass (M_H) and Total and Wide Jet Broadening (B_T and B_W) which are defined in reference [1] and references therein.

The data distributions for T, T_{major}, T_{minor}, O, S and A are shown in Figure 2 and for C, M_H, B_T and B_W are shown in Figure 3. The predictions of the PYTHIA, HERWIG 5.9[3] [14], ARIADNE and COJETS Monte Carlo models are also shown. Numerical values for the data are given in Tables 1– 5. Within the uncertainties, the Monte Carlo predictions of PYTHIA, HERWIG and ARIADNE are seen to be in overall agreement with the data. COJETS predicts a T_{minor} distribution which lies somewhat above the data points for central T_{minor} values, and an O distribution which lies somewhat below the data points for central O values, but is otherwise in general agreement with the data.

We also study the event shape observables by computing their mean, width σ, and skewness $\gamma = m_3/\sigma^3$, where $m_3 = \langle (x - \langle x \rangle)^3 \rangle$ for a generic distribution x. The results are given in Table 6 for data and for PYTHIA, HERWIG, ARIADNE and COJETS. In Figure 4 the differences for mean, width and skewness between the Monte Carlo predictions and the data are shown. We find reasonable agreement of the Monte Carlo predictions with the data at the level of one to two standard deviations of the total uncertainties, except for the COJETS prediction for the mean of T_{minor}. The differences between data and Monte Carlo are correlated between the various event shape observables. In general, the Monte Carlo distributions describe the data well but have a slightly larger mean, are somewhat wider and are more skewed than the data.

The mean value of the Thrust distribution is shown in Figure 5 together with data from lower energy measurements [1–4, 25] and the predictions for the energy evolution from PYTHIA, HERWIG, ARIADNE and COJETS. The predictions of all four Monte Carlo models are consistent with our new measurement.

5.2 Jet production rates

We measure the jet production rates using two recombination jet finding algorithms, the JADE (E0) [26] and Durham (D) [23] schemes, and two variations of a cone jet algorithm [27], all of which are implemented as described in our previous publication and references therein [1].

As in previous analyses [1, 10] we define the differential 2-jet rate $D_2 = \mathrm{d}R_2/\mathrm{d}y_{\mathrm{cut}}$, where R_2 is the 2-jet rate and y_{cut} the jet resolution parameter. For the cone jet algorithm we replace the minimum cone energy, ε, by $\varepsilon' = \varepsilon \cdot E_{\mathrm{vis}}/\sqrt{s}$, where E_{vis} is the sum of the energies of all particles used in the jet finding. In our studies the jet rates are computed at fixed $\varepsilon = 7$ GeV as R is varied or at fixed $R = 0.7$ radians as ε is varied.

Figure 6 shows the jet rates for the E0, D and cone schemes, versus their resolution parameters. Numerical values for these data are given in Tables 7 to 10. There are strong bin to bin correlations. The data are compared with the predictions of PYTHIA, HERWIG, COJETS and ARIADNE. The Monte Carlo predictions show in general good agreement with the data. For the E0 and the D scheme the 3-jet rate according to COJETS tends to be somewhat smaller than the other predictions at small values of the resolution parameter, but still is consistent with the data. For the two variants of the cone algorithm, the Monte Carlo predictions are in good agreement with the data. The

[3]For comparison at the hadron-level we use version 5.9 of HERWIG with one parameter changed relative to our standard tuning [13], in order to improve the model's description of the mean charged particle multiplicity at the Z^0: Maximum cluster mass CLMAX = 3.75.

differential 2-jet rate D_2 for the D scheme is shown in Figure 3 and tabulated in Table 11. The mean, width and skewness values for this distribution are given in Table 6 and are shown in comparison to the Monte Carlo predictions in figure 4. The D_2 distribution is well described by the Monte Carlo models (see Figure 3).

The 3-jet rate measured with the E0 scheme at $y_{\mathrm{cut}} = 0.08$, published by many experiments, shows the running of the strong coupling strength in a particularly direct manner [28]. In Figure 7 we show this rate at a c.m. energy of 161 GeV together with measurements at lower e^+e^- c.m. energies [1,3,30]. The curve is a fit of the $\mathcal{O}(\alpha_s^2)$ QCD prediction [31] for the evolution of R_3 with c.m. energy to the data from 22 GeV to 133 GeV [1,32] and to our measurement at 161 GeV. The fit, mostly sensitive to lower energy data, has a central value of $\alpha_s(M_{Z^0}) = 0.121$, with $\chi^2/\mathrm{d.o.f.} = 1.0$, where the statistical error from the fit is negligible.

5.3 Determination of α_s

Our measurement of the strong coupling strength $\alpha_s(161\ \mathrm{GeV})$ is based on fits of the QCD predictions to the corrected distributions for $1-T$, M_H, B_T, B_W and D_2, with the D_2 distribution defined using the Durham jet scheme. The theoretical descriptions of these five observables are the most complete, allowing the use of combined $\mathcal{O}(\alpha_s^2)$+NLLA QCD calculations [33–35]. We note that for the D_2 distribution, $\mathcal{O}(\alpha_s^2)$+NLLA calculations are currently available only using the Durham scheme. We follow the procedures described in reference [1,10] as closely as possible in order to obtain results which we can compare directly to our previous analysis. In particular, we choose the so-called $\ln(R)$-matching scheme, and fix the renormalisation scale parameter, $x_\mu \equiv \mu/\sqrt{s}$, to $x_\mu = 1$, where μ is the energy scale at which the theory is renormalised.

Analytic QCD predictions describe distributions at the level of quarks and gluons (parton level). The predictions are convolved with hadronisation effects by multiplying by the ratio of hadron- to parton-level cumulative distributions determined using a Monte Carlo model. We use PYTHIA to generate events at $\sqrt{s} = 161.0$ GeV for this purpose. The resulting cumulative distributions are used to obtain differential distributions with the same binning as the data.

The fit ranges are determined by the following considerations. For each observable, the ratio between Monte Carlo distributions computed for partons and hadrons is required to be unity to within about 10%, the fit ranges are required to be similar to the fit ranges used in our studies at $\sqrt{s} = M_{Z^0}$ and 133 GeV [1,10], and the distribution of partons from Monte Carlo models is required to be well described by the analytic predictions.

We find satisfactory fits for all five observables with $\chi^2/\mathrm{d.o.f.}$ of the fits generally not much larger than unity. The results are given in Table 12 and in Figure 8. The statistical uncertainties are estimated from the variance of α_s values derived from fits to 100 independent sets of simulated events, each with about the same number of events as the data.

The experimental uncertainty is defined by the quadratic sum of: the largest difference between the central result and the results from tracks or clusters only; the difference found when using the alternative selection; and the difference from using the additional cut on M_{W}^{fit} to reject 4-fermion events. The same procedure as described in section 4.3 is used to estimate and subtract statistical fluctuations in the systematic terms defined for the analysis. The experimental uncertainties are shown in Table 12 and are about the same size as the statistical uncertainties.

The hadronisation uncertainty is defined by adding in quadrature: the larger of the changes in α_s observed when varying the hadronisation parameters b and σ_Q by $\pm$ 1 standard deviation about their tuned values [13] in PYTHIA; the change observed when the parton virtuality cutoff parameter is altered from $Q_0 = 1.9$ GeV to $Q_0 = 4$ GeV in PYTHIA, corresponding to a change of the mean parton multiplicity from 7.0 to 4.8; the change observed when on the parton level only the light quarks u, d, s and c are considered in order to estimate potential quark mass effects; and both differences with respect to the standard result when HERWIG 5.9 or ARIADNE are used to account for the hadronization effects, rather than PYTHIA. For all observables the hadronisation uncertainties, given in Table 12, are relatively small compared to the statistical or experimental systematic errors.

In estimating the hadronization uncertainty on α_s, we do not consider COJETS. This is because the parton shower in this model contains only 3.9 partons on average. It thus does not match well with the NLLA calculations which are valid for multipartonic final states. In particular the large fraction of events which contain only two partons is in clear disagreement with these predictions. A similar strategy was adopted in references [36,37].

The importance of uncomputed higher order terms in the theory may be estimated by studying the effects of varying the renormalisation scale parameter x_μ. We estimate the dependence of our fit results on the renormalisation scale x_μ as in references [1,10], by repeating the fits using $x_\mu = 0.5$ and $x_\mu = 2$. We find variations which are generally smaller than the statistical uncertainties and which are highly correlated between all observables. We treat the variation of the scale x_μ as an asymmetric uncertainty on α_s.

The total uncertainty for each individual observable is computed by adding in quadrature the statistical, the experimental, the hadronisation and the scale uncertainties. The total uncertainty on α_s(161 GeV) is typically around 10%. The D_2 distribution has particularly small experimental and renormalisation scale uncertainties and yields the smallest total uncertainty for α_s of any of the distributions.

We also derive a combined result for the strong coupling strength at 161 GeV using the weighted average procedure as described in reference [10]. The statistical uncertainty of the combined result is estimated using 100 independent samples of Monte Carlo events in the same manner as for the individual measurements. Our final result is

$$\alpha_s(161 \text{ GeV}) = 0.101 \pm 0.005(\text{stat.}) \pm 0.007(\text{syst.}). \tag{1}$$

The systematic uncertainty has contributions from experimental effects (± 0.006), hadronisation effects (± 0.002) and from variations of the renormalisation scale (± 0.003), defined as explained above for the individual distributions. This result leads to $\alpha_s(M_{Z^0}) = 0.109 \pm 0.010$ when evolved to the scale of M_{Z^0}. For comparison, our measurements at the M_{Z^0} energy with a slightly larger set of observables based on $\mathcal{O}(\alpha_s^2)$+NLLA QCD calculations yielded $\alpha_s(M_{Z^0}) = 0.120 \pm 0.006$ [10]. In order to compare average α_s values using exactly the same theoretical predictions and observables, we compute the weighted average from our present fits to $1-T$, M_H, B_T and B_W which yields $\alpha_s(161 \text{ GeV}) = 0.101 \pm 0.009$ ($\alpha_s(M_{Z^0}) = 0.109 \pm 0.010$). Our previous analysis at

$\sqrt{s} = M_{Z^0}$ gave $\alpha_s(M_{Z^0}) = 0.116 \pm 0.006$ from fits of the same predictions to the same observables. Our present determination of α_s is therefore consistent with our measurement at $\sqrt{s} = M_{Z^0}$.

In Figure 9 [28, 29] we show our measurement (1) together with other measurements of the strong coupling strength, as a function of the energy scale Q. The curve shows the $\mathcal{O}(\alpha_s^3)$ prediction for $\alpha_s(Q)$ using $\alpha_s(M_{Z^0}) = 0.118 \pm 0.006$ as given in reference [28]. Our measurement of $\alpha_s(161 \text{ GeV})$ is consistent with the running of α_s required by QCD.

5.4 Charged particle momentum spectra

We measure the charged particle fragmentation function, $1/\sigma \cdot \mathrm{d}\sigma_{\mathrm{ch}}/\mathrm{d}x_p$, and the ξ_p distribution, $1/\sigma \cdot \mathrm{d}\sigma_{\mathrm{ch}}/\mathrm{d}\xi_p$, where $x_p = 2p/\sqrt{s}$, $\xi_p = \ln(1/x_p)$ and p is the measured track momentum, using the same methods as in our previous publication [1]. We also study the distribution of rapidity, y, relative to the Thrust axis and the distributions of the track momentum components parallel, $p_\perp^{\mathrm{in}}$, and perpendicular, $p_\perp^{\mathrm{out}}$, to the event plane. This plane is defined by the eigenvectors of the momentum tensor associated with the two largest eigenvalues, as in reference [1].

The $p_\perp^{\mathrm{in}}$, $p_\perp^{\mathrm{out}}$ and y distributions are shown in Figures 10 and 11 (a). The data are tabulated in Tables 13 and 14. We observe good agreement between PYTHIA, HERWIG and ARIADNE and the data for the two $p_\perp$ distributions. However, the slope of the $p_\perp^{\mathrm{in}}$ distribution of the COJETS prediction is somewhat steeper for large $p_\perp^{\mathrm{in}}$ than the data whereas the $p_\perp^{\mathrm{out}}$ distribution is described relatively well by this model. In the y distribution, there is reasonable agreement of the PYTHIA, HERWIG and ARIADNE Monte Carlo models with the data once the different charged particle multiplicities in data and Monte Carlo are taken into account (see section 5.5). The COJETS Monte Carlo model overestimates the production of charged particles with low values of y.

The fragmentation function and the ξ_p distribution are shown in Figures 11 (b) and 12 (a) together with the Monte Carlo predictions. Numerical values of these data are given in Tables 15 and 16. The spectrum of charged particles with large momentum fraction x_p is well described by all Monte Carlo models. The shape of the ξ_p distribution is well described by PYTHIA, HERWIG and ARIADNE, although their normalisation is somewhat higher. The COJETS Monte Carlo predicts too many particles in the region of the peak and at large values of ξ_p, where low momentum particles contribute. In the LLA approach, this is the region where soft gluon production is reduced as a consequence of destructive interference.

Using the assumption of local parton hadron duality (LPHD), the leading-log approximation of QCD calculations (LLA) predicts the shape of the ξ_p distribution to be Gaussian. The peak of the distribution is predicted to have an almost logarithmic variation with energy. The NLLA QCD calculations [38] predict the shape to be a Gaussian with higher moments (skewed Gaussian), and the same energy dependence of the peak as the LLA. We fit a skewed Gaussian to the region close to the peak of the ξ_p distribution and determine the position of the peak, ξ_0, to be

$$\xi_0(161 \text{ GeV}) = 4.00 \pm 0.03(\text{stat.}) \pm 0.02(\text{syst.}), \tag{2}$$

The systematic error is detailed in Table 17. Unlike reference [1], we do not include an uncertainty on ξ_0 from fitting a simple Gaussian to the ξ_p distribution, since a simple Gaussian represents the LLA of QCD only. In Figure 12 (b) we show our measurement of ξ_0 together with measurements taken at lower c.m. energies [1,2,4,39] and a fit of the NLLA prediction to the lower energy data up to and including $\sqrt{s} = 133$ GeV. The value of the NLLA prediction extrapolated to $\sqrt{s} = 161$ GeV, 3.93 ± 0.01, is lower than our measurement at 161 GeV by about two standard deviations. As noted in our previous publication [1], the fit is dominated by contributions from the data points with small errors at 29 and 35 GeV.

In the modified leading-log approximation (MLLA) [40], the most complete calculation available, the ξ_p distribution is predicted in terms of two parameters, a QCD scale Λ and a normalisation factor $K(\sqrt{s})$ associated with the LPHD hypothesis which has a weak c.m. energy dependence due to the approximate nature of the LPHD. The values of $K(\sqrt{s})$ obtained in reference [41] are consistent with a linear c.m. energy variation. A fit of the MLLA prediction for the ξ_p distribution to OPAL data recorded at a c.m. energy of 91 GeV [41] determined Λ and $K(M_{Z^0})$. Figure 12 (a) shows the prediction of the MLLA at $\sqrt{s} = 161$ GeV as a shaded band, using the result for Λ from reference [41]. The upper edge of the band corresponds to $K(161 \text{ GeV}) = K(M_{Z^0})$ whereas the lower edge corresponds to $K(161 \text{ GeV}) = 1.16$ (extrapolated from the values in reference [41] using the linear c.m. variation mentioned above). The description of the data around the peak is relatively good for the extrapolated value of $K(161 \text{ GeV})$, considering that there are no free parameters. The MLLA prediction is not very different from the predictions of PYTHIA and HERWIG, except at large ξ_p where kinematic effects become important and where the perturbative QCD calculations are not valid. The curve for the ARIADNE prediction is almost indistinguishable from the PYTHIA prediction and is omitted.

5.5 Charged particle multiplicity

Finally, we measure the charged particle multiplicity distribution and derive several related quantities from it. In particular, we evaluate the mean charged multiplicity $\langle n_{\text{ch}} \rangle$, the dispersion $D = (\langle n_{\text{ch}}^2 \rangle - \langle n_{\text{ch}} \rangle^2)^{\frac{1}{2}}$, the ratio $\langle n_{\text{ch}} \rangle / D$, the normalised second moment $C_2 = \langle n_{\text{ch}}^2 \rangle / \langle n_{\text{ch}} \rangle^2$ and the second binomial moment $\mathcal{R}_2 = \langle n_{\text{ch}}(n_{\text{ch}} - 1) \rangle / \langle n_{\text{ch}} \rangle^2$.

To correct the charged particle multiplicity distribution, we subtract the expected background from 4-fermion events as described in section 4.2. The resulting distribution is corrected for experimental effects such as acceptance, resolution and secondary interactions in the detector with an unfolding matrix, as previously done in reference [1]. This matrix is determined from the PYTHIA sample of fully simulated $(Z^0/\gamma)^*$ events. Biases introduced by the event selection and by residual ISR are corrected using a bin-by-bin multiplication method. The bin-by-bin corrections are typically smaller than 10–15%.

The corrected charged particle multiplicity distribution is shown in Figure 13 (a). Numerical values for the data are given in Table 18. The COJETS model predicts too many high multiplicity events and clearly disagrees with the data. Since COJETS provides a good description of the charged particle multiplicity distribution at $\sqrt{s} \sim M_{Z^0}$, this suggests that the energy scaling behaviour of COJETS is inaccurate. The PYTHIA, HERWIG and ARIADNE models describe the data reasonably well.

We determine the mean value, the dispersion and the higher multiplicity moments to be:

$$\begin{aligned}
\langle n_{\mathrm{ch}}\rangle(161\ \mathrm{GeV}) &= 24.46 \pm 0.45(\mathrm{stat.}) \pm 0.44(\mathrm{syst.}), \\
D(161\ \mathrm{GeV}) &= 7.68 \pm 0.37(\mathrm{stat.}) \pm 0.30(\mathrm{syst.}), \\
\langle n_{\mathrm{ch}}\rangle / D(161\ \mathrm{GeV}) &= 3.19 \pm 0.14(\mathrm{stat.}) \pm 0.11(\mathrm{syst.}), \\
C_2(161\ \mathrm{GeV}) &= 1.099 \pm 0.009(\mathrm{stat.}) \pm 0.007(\mathrm{syst.}) \ \text{and} \\
\mathcal{R}_2(161\ \mathrm{GeV}) &= 1.058 \pm 0.009(\mathrm{stat.}) \pm 0.007(\mathrm{syst.}).
\end{aligned} \tag{3}$$

The systematic uncertainties are estimated in the same manner as described in section 4.3 and are listed in Table 17. The analysis was repeated with data recorded at the Z^0 peak in 1996 to check for possible deviations of the detector response with respect to previous years. We found $\langle n_{\mathrm{ch}}\rangle(M_{Z^0}) = 20.83 \pm 0.08(\mathrm{stat.})$, which is consistent with the value of $\langle n_{\mathrm{ch}}\rangle(M_{Z^0})$ we obtained by integrating the longitudinal fragmentation function, $\langle n_{\mathrm{ch}}\rangle(M_{Z^0}) = 21.05 \pm 0.01(\mathrm{stat.}) \pm 0.20(\mathrm{syst.})$ [42].

Alternatively, the mean charged multiplicity is computed by integrating the corrected rapidity distribution, or the fragmentation function (see Table 17). Both the rapidity distribution and the fragmentation function give a result consistent with the one from the direct measurement presented in this section. For example, the result found by integrating the fragmentation function is $\langle n_{\mathrm{ch}}\rangle(161\ \mathrm{GeV}) = 24.24 \pm 0.43(\mathrm{stat.}) \pm 0.55(\mathrm{syst.})$.

We compare our results with data recorded at lower c.m. energies and with analytic QCD or Monte Carlo predictions. The dispersion and higher moments are consistent with measurements made at lower c.m. energies [1,43], in agreement with the QCD Monte Carlo and analytic (where available) predictions. The predicted values of $\langle n_{\mathrm{ch}}\rangle(161\ \mathrm{GeV})$ from PYTHIA and ARIADNE are 25.9, while that from HERWIG 5.9 is 25.5, all of which are about two standard deviations of the total uncertainty above our measurement. COJETS predicts a value of 28.3, which differs by 6 standard deviations from our measurement. Figure 13 (b) shows our measurement of $\langle n_{\mathrm{ch}}\rangle$ as well as those obtained at energies from 12 to 136 GeV [1–3,5,42,44]. The dash-dotted curve shows the NLLA QCD prediction [45] for the energy evolution of the charged particle multiplicity, with parameters fitted to all data points between 12 and 136 GeV. The NLLA calculation predicts a mean charged multiplicity at 161 GeV of 26.0 ± 0.2, about 2.4 standard deviations above our measurement. Variations in the quark flavour composition at the different c.m. energies do not significantly influence the results of the fit.

6 Summary and conclusions

In this paper we have presented measurements of the properties of hadronic events produced at LEP at a centre-of-mass energy of 161 GeV. We have determined the corrected distributions for event shape observables, for jet rates using different jet finding algorithms, for the charged particle multiplicity and for charged particle momentum spectra. The predictions of the PYTHIA, HERWIG and ARIADNE Monte Carlo models are found to be in general agreement with the measured distributions, although their prediction for the mean charged particle multiplicity is above our measurement by about two standard deviations of the total uncertainty. The COJETS Monte Carlo model describes the event shape distributions well, but overestimates the production of soft charged particles in the rapidity, $\xi_p = \ln(1/x_p)$ and $n_{\rm ch}$ distributions.

From a fit of $\mathcal{O}(\alpha_s^2)$+NLLA QCD predictions to four event shape distributions and the differential two jet rate distribution, defined using the Durham jet finder, we have determined the strong coupling strength to be $\alpha_s(161\ \mathrm{GeV}) = 0.101 \pm 0.005(\mathrm{stat.}) \pm 0.007(\mathrm{syst.})$. If this measurement is evolved to the Z^0 peak it results in $\alpha_s(M_{\mathrm{Z}^0}) = 0.109 \pm 0.010$ which may be directly compared to our previous measurement of $\alpha_s(M_{\mathrm{Z}^0}) = 0.116 \pm 0.006$ using the same set of observables and $\mathcal{O}(\alpha_s^2)$+NLLA QCD predictions.

The ξ_p distribution has been found to be reasonably well described by QCD NLLA and MLLA calculations, and the position of the peak was measured to be $\xi_0(161\ \mathrm{GeV}) = 4.00 \pm 0.03(\mathrm{stat.}) \pm 0.02(\mathrm{syst.})$. This is in fair agreement with the expectation for the energy evolution given by QCD NLLA calculations.

The mean charged particle multiplicity has been determined to be $\langle n_{\rm ch}\rangle(161\ \mathrm{GeV}) = 24.46 \pm 0.45(\mathrm{stat.}) \pm 0.44(\mathrm{syst.})$, about two standard deviations below the NLLA QCD predictions and the PYTHIA, HERWIG and ARIADNE Monte Carlo predictions. We have also determined the dispersion and second multiplicity moments, which are found to be consistent with values determined at lower c.m. energies, in agreement with expectations.

Our studies show that most of the features of hadronic events produced in $\mathrm{e}^+\mathrm{e}^-$ collisions at energies above the Z^0 mass are well described by QCD either in the form of analytic or Monte Carlo predictions. Further tests of QCD at yet higher $\mathrm{e}^+\mathrm{e}^-$ energies with increased precision will soon be possible with the continuation of the LEP 2 programme.

Acknowledgements

We particularly wish to thank the SL Division for the efficient operation of the LEP accelerator at the new energy of $\sqrt{s} = 161$ GeV and for their continuing close cooperation with our experimental group. We thank our colleagues from CEA, DAPNIA/SPP, CE-Saclay for their efforts over the years on the time-of-flight and trigger systems which we continue to use. In addition to the support staff at our own institutions we are pleased to acknowledge the
Department of Energy, USA,
National Science Foundation, USA,
Particle Physics and Astronomy Research Council, UK,
Natural Sciences and Engineering Research Council, Canada,
Israel Science Foundation, administered by the Israel Academy of Science and Humanities,
Minerva Gesellschaft,
Japanese Ministry of Education, Science and Culture (the Monbusho) and a grant under the Monbusho International Science Research Program,
German Israeli Bi-national Science Foundation (GIF),
Bundesministerium für Bildung, Wissenschaft, Forschung und Technologie, Germany,

National Research Council of Canada,
Hungarian Foundation for Scientific Research, OTKA T-016660, and OTKA F-015089.

References

[1] OPAL Coll., G. Alexander et al.: Z. Phys. C 72 (1996) 191

[2] ALEPH Coll., D. Buskulic et al.: CERN-PPE/96-043 (1996), Sub. to Z. Phys. C

[3] L3 Coll., M. Acciarri et al.: Phys. Lett. B 371 (1996) 137

[4] DELPHI Coll., P. Abreu et al.: CERN-PPE/96-130 (1996), Sub. to Z. Phys. C

[5] DELPHI Coll., P. Abreu et al.: Phys. Lett. B 372 (1996) 172

[6] S. Bethke and J.E. Pilcher: Annu. Rev. Nucl. Part. Sci. 42 (1992) 251

[7] OPAL Coll., K. Ahmet et al.: Nucl. Instrum. Methods A 305 (1991) 275

[8] LEP Energy Working Group Internal Note 97-01 (in preparation)

[9] OPAL Coll., G. Alexander et al.: Z. Phys. C 52 (1991) 175

[10] OPAL Coll., P. D. Acton et al.: Z. Phys. C 59 (1993) 1

[11] J. Allison et al.: Nucl. Instrum. Methods A 317 (1992) 47

[12] T. Sjöstrand: Comput. Phys. Commun. 82 (1994) 74

[13] OPAL Coll., G. Alexander et al.: Z. Phys. C 69 (1996) 543

[14] G. Marchesini et al.: Comput. Phys. Commun. 67 (1992) 465

[15] J. Fujimoto et al.: KEK-CP-046 (1996), to appear in Comput. Phys. Commun.

[16] Particle Data Group Coll., R. M. Barnett et al.: Phys. Rev. D 54 (1996) 1

[17] D. Bardin et al.: Nucl. Phys. Proc. Suppl. B 37 (1994) 148

[18] F.A. Berends, R. Pittau and R. Kleiss: Comput. Phys. Commun. 85 (1995) 437

[19] L. Lönnblad: Comput. Phys. Commun. 71 (1992) 15

[20] R. Odorico, Comp. Phys. Comm. 72 (1992) 238.

[21] P. Mazzanti and R. Odorico: Nucl. Phys. B 394 (1993) 267

[22] OPAL Coll., G. Alexander et al.: Phys. Lett. B 376 (1996) 232

[23] S. Catani et al.: Nucl. Phys. B 269 (1991) 432

[24] OPAL Coll., K. Ackerstaff et al.: Phys. Lett. B 389 (1996) 416.

[25] TASSO Coll., W. Braunschweig et al.: Z. Phys. C 47 (1990) 187
AMY Coll., Y. Li et al.: Phys. Rev. D 41 (1990) 2675
ALEPH Coll., D. Buskulic et al.: Z. Phys. C 55 (1992) 209
DELPHI Coll., D. Aarnio et al.: Phys. Lett. B 240 (1990) 271
L3 Coll., B. Adeva et al.: Z. Phys. C 55 (1992) 39

[26] JADE Coll., W. Bartel et al.: Z. Phys. C 33 (1986) 23

[27] OPAL Coll., R. Akers et al.: Z. Phys. C 63 (1994) 197

[28] S. Bethke: PITHA 96/30 (1996), Talk presented at the QCD Euroconference 96, Montpellier, France, July 4-12 (1996)

[29] M. Schmelling, Talk presented at the International Conference on High Energy Physics, Warsaw, Poland, July 25-31 (1996)

[30] JADE Coll., S. Bethke et al.: Phys. Lett. B 213 (1988) 235
JADE Coll., W. Bartel et al.: Z. Phys. C 33 (1986) 23
MARK II Coll., S. Bethke et al.: Z. Phys. C 43 (1989) 325
MARK II Coll., G. Abrams et al.: Phys. Rev. Lett. 63 (1989) 1558
TASSO Coll., W. Braunschweig et al.: Phys. Lett. B 214 (1988) 286
AMY Coll., I. Park et al.: Phys. Rev. Lett. 62 (1989) 1713
L3 Coll., B. Adeva et al.: Phys. Lett. B 248 (1990) 464
OPAL Coll., M. Akrawy et al.: Z. Phys. C 49 (1991) 375

[31] S. Bethke, Z. Kunszt, D.E. Soper and W.J. Stirling: Nucl. Phys. B 370 (1992) 310

[32] OPAL Coll., M. Z. Akrawy et al.: Phys. Lett. B 235 (1990) 389

[33] S. Catani, L. Trentadue, G. Turnock and B.R. Webber: Nucl. Phys. B 407 (1993) 3

[34] S. Catani, G. Turnock and B.R. Webber: Phys. Lett. B 295 (1992) 269

[35] G. Dissertori and M. Schmelling: Phys. Lett. B 361 (1995) 167

[36] OPAL Coll., P. Acton et al.: Phys. Lett. B 276 (1992) 547

[37] OPAL Coll., P. Acton et al.: Z. Phys. C 55 (1992) 1

[38] C.P. Fong and B.R. Webber: Nucl. Phys. B 355 (1991) 54

[39] TASSO Coll., W. Braunschweig et al.: Z. Phys. C 47 (1990) 187
MARK II Coll., A. Petersen et al.: Phys. Rev. D 37 (1988) 1
TPC Coll., H. Aihara et al.: LBL-23727 (1988)
AMY Coll., Y. Li et al.: Phys. Rev. D 411 (1990) 2675
ALEPH Coll., D. Buskulic et al.: Z. Phys. C 55 (1992) 209
DELPHI Coll., P. Abreu et al.: Phys. Lett. B 275 (1992) 231
L3 Coll., B. Adeva et al.: Phys. Lett. B 229 (1991) 199

[40] V. A. Khoze, Yu. L. Dokshitzer and S. I. Troyan: Int. J. Mod. Phys. A 7 (1992) 1875

[41] OPAL Coll., M. Z. Akrawy et al.: Phys. Lett. B 247 (1990) 617

[42] OPAL Coll., R. Akers et al.: Z. Phys. C 68 (1995) 203

[43] M. Schmelling: Physica Scripta 51 (1995) 683

[44] JADE Coll., W. Bartel et al.: Z. Phys. C 20 (1983) 187
TASSO Coll., W. Braunschweig et al.: Z. Phys. C 45 (1989) 193
TPC Coll., H. Aihara et al.: Phys. Lett. B 134 (1987) 299
HRS Coll., M. Derrick et al.: Phys. Rev. D 34 (1986) 3304
AMY Coll., H. Zheng et al.: Phys. Rev. D 42 (1990) 737
MARK II Coll., G. Abrams et al.: Phys. Rev. Lett. 64 (1990) 1334
ALEPH Coll., D. Buskulic et al.: Z. Phys. C 69 (1995) 15
DELPHI Coll., P. Abreu et al.: Z. Phys. C 50 (1991) 185
L3 Coll., B. Adeva et al.: Z. Phys. C 55 (1992) 39

[45] B.R. Webber: Phys. Lett. B 143 (1984) 501

Tables

T	$1/\sigma \cdot \mathrm{d}\sigma/\mathrm{d}T$
0.70 – 0.78	0.14 ± 0.12 ± 0.47
0.78 – 0.85	0.93 ± 0.24 ± 0.47
0.85 – 0.88	1.02 ± 0.39 ± 0.61
0.88 – 0.91	3.10 ± 0.64 ± 0.59
0.91 – 0.93	3.56 ± 0.82 ± 0.81
0.93 – 0.95	3.92 ± 0.84 ± 1.29
0.95 – 0.96	6.5 ± 1.5 ± 1.4
0.96 – 0.97	10.1 ± 1.9 ± 1.6
0.97 – 0.98	18.1 ± 2.5 ± 2.6
0.98 – 0.99	22.1 ± 2.9 ± 2.6
0.99 – 1.00	8.6 ± 1.7 ± 2.6

T_{major}	$1/\sigma \cdot \mathrm{d}\sigma/\mathrm{d}T_{\mathrm{major}}$
0.000 – 0.040	0.55 ± 0.25 ± 0.43
0.040 – 0.080	6.80 ± 0.81 ± 0.43
0.080 – 0.120	5.89 ± 0.69 ± 0.41
0.120 – 0.160	3.07 ± 0.51 ± 0.27
0.160 – 0.220	1.95 ± 0.34 ± 0.10
0.220 – 0.300	1.36 ± 0.26 ± 0.12
0.300 – 0.400	0.92 ± 0.20 ± 0.13
0.400 – 0.500	0.33 ± 0.13 ± 0.13

Table 1: Measured values for the Thrust T and Thrust Major T_{major} distributions. The first error is statistical, the second systematic.

T_{minor}	$1/\sigma \cdot \mathrm{d}\sigma/\mathrm{d}T_{\mathrm{minor}}$
0.020 – 0.040	9.2 ± 1.3 ± 0.8
0.040 – 0.060	16.4 ± 1.8 ± 1.3
0.060 – 0.080	9.5 ± 1.3 ± 2.2
0.080 – 0.100	6.1 ± 1.0 ± 1.8
0.100 – 0.120	3.11 ± 0.74 ± 1.51
0.120 – 0.140	1.40 ± 0.53 ± 0.66
0.140 – 0.160	1.61 ± 0.58 ± 0.58
0.160 – 0.200	0.87 ± 0.31 ± 0.35
0.200 – 0.240	0.23 ± 0.19 ± 0.21
0.240 – 0.300	0.14 ± 0.13 ± 0.21

O	$1/\sigma \cdot \mathrm{d}\sigma/\mathrm{d}O$
0.000 – 0.050	9.77 ± 0.83 ± 0.28
0.050 – 0.100	4.58 ± 0.57 ± 0.28
0.100 – 0.150	2.22 ± 0.42 ± 0.27
0.150 – 0.200	1.24 ± 0.32 ± 0.25
0.200 – 0.250	1.14 ± 0.31 ± 0.32
0.250 – 0.300	0.67 ± 0.24 ± 0.29
0.300 – 0.400	0.23 ± 0.12 ± 0.29

Table 2: Measured values for the Thrust Minor T_{minor} and Oblateness O distributions. The first error is statistical, the second systematic.

S	$1/\sigma \cdot \mathrm{d}\sigma/\mathrm{d}S$
0.000 – 0.020	28.1 ± 2.1 ± 2.5
0.020 – 0.040	5.3 ± 1.0 ± 2.5
0.040 – 0.060	3.19 ± 0.80 ± 1.66
0.060 – 0.120	1.98 ± 0.38 ± 1.06
0.120 – 0.200	1.06 ± 0.25 ± 0.25
0.200 – 0.300	0.43 ± 0.16 ± 0.21
0.300 – 0.500	0.12 ± 0.07 ± 0.21

A	$1/\sigma \cdot \mathrm{d}\sigma/\mathrm{d}A$
0.000 – 0.005	129.7 ± 9.3 ± 5.0
0.005 – 0.010	33.7 ± 5.4 ± 5.0
0.010 – 0.015	8.1 ± 2.9 ± 4.1
0.015 – 0.025	8.1 ± 2.0 ± 3.0
0.025 – 0.040	2.6 ± 1.0 ± 1.1
0.040 – 0.070	0.54 ± 0.36 ± 0.46
0.070 – 0.100	0.11 ± 0.23 ± 0.46

Table 3: Measured values for the Sphericity S and Aplanarity A distributions. The first error is statistical, the second systematic.

C	$1/\sigma \cdot \mathrm{d}\sigma/\mathrm{d}C$
0.000 – 0.050	1.92 ± 0.37 ± 0.22
0.050 – 0.080	5.04 ± 0.81 ± 0.22
0.080 – 0.110	4.59 ± 0.74 ± 0.12
0.110 – 0.140	3.37 ± 0.61 ± 0.17
0.140 – 0.180	2.40 ± 0.45 ± 0.21
0.180 – 0.220	1.63 ± 0.37 ± 0.19
0.220 – 0.300	1.17 ± 0.23 ± 0.11
0.300 – 0.400	0.77 ± 0.17 ± 0.08
0.400 – 0.500	0.91 ± 0.19 ± 0.14
0.500 – 0.600	0.58 ± 0.16 ± 0.14
0.600 – 0.750	0.20 ± 0.09 ± 0.07
0.750 – 1.000	0.01 ± 0.04 ± 0.07

M_H	$1/\sigma \cdot \mathrm{d}\sigma/\mathrm{d}M_H$
0.060 – 0.075	1.79 ± 0.43 ± 1.24
0.075 – 0.090	2.28 ± 0.62 ± 1.24
0.090 – 0.110	7.8 ± 1.2 ± 1.2
0.110 – 0.140	6.49 ± 0.94 ± 0.86
0.140 – 0.170	4.80 ± 0.77 ± 0.91
0.170 – 0.200	3.54 ± 0.67 ± 0.85
0.200 – 0.250	2.09 ± 0.41 ± 0.89
0.250 – 0.300	2.45 ± 0.45 ± 0.84
0.300 – 0.350	0.97 ± 0.31 ± 0.61
0.350 – 0.450	0.59 ± 0.18 ± 0.26
0.450 – 0.600	0.02 ± 0.04 ± 0.26

Table 4: Measured values for the C-parameter C and Heavy Jet Mass M_H distributions. The first error is statistical, the second systematic.

B_T	$1/\sigma \cdot \mathrm{d}\sigma/\mathrm{d}B_T$
0.000 – 0.030	2.1 $\pm$ 0.5 $\pm$ 1.0
0.030 – 0.040	7.4 $\pm$ 1.8 $\pm$ 1.0
0.040 – 0.050	14.1 $\pm$ 2.3 $\pm$ 1.2
0.050 – 0.060	12.7 $\pm$ 2.1 $\pm$ 1.1
0.060 – 0.075	8.7 $\pm$ 1.4 $\pm$ 1.2
0.075 – 0.090	6.6 $\pm$ 1.2 $\pm$ 1.3
0.090 – 0.110	4.09 $\pm$ 0.84 $\pm$ 0.86
0.110 – 0.130	2.20 $\pm$ 0.64 $\pm$ 0.53
0.130 – 0.160	2.62 $\pm$ 0.56 $\pm$ 0.29
0.160 – 0.200	2.23 $\pm$ 0.47 $\pm$ 0.22
0.200 – 0.250	1.29 $\pm$ 0.33 $\pm$ 0.22
0.250 – 0.300	0.23 $\pm$ 0.19 $\pm$ 0.22

B_W	$1/\sigma \cdot \mathrm{d}\sigma/\mathrm{d}B_W$
0.000 – 0.020	4.7 $\pm$ 1.0 $\pm$ 1.6
0.020 – 0.030	16.6 $\pm$ 2.5 $\pm$ 1.6
0.030 – 0.040	16.5 $\pm$ 2.3 $\pm$ 1.8
0.040 – 0.050	10.2 $\pm$ 1.8 $\pm$ 1.2
0.050 – 0.065	8.2 $\pm$ 1.4 $\pm$ 0.9
0.065 – 0.080	5.7 $\pm$ 1.2 $\pm$ 0.9
0.080 – 0.100	1.89 $\pm$ 0.62 $\pm$ 0.83
0.100 – 0.150	3.09 $\pm$ 0.50 $\pm$ 0.68
0.150 – 0.200	1.22 $\pm$ 0.36 $\pm$ 0.35
0.200 – 0.250	0.22 $\pm$ 0.17 $\pm$ 0.15
0.250 – 0.300	0.02 $\pm$ 0.05 $\pm$ 0.15

Table 5: Measured values for the Total B_T and Wide B_W Jet Broadening distributions. The first error is statistical, the second systematic.

	Data	PYTHIA	HERWIG	COJETS	ARIADNE
	Mean				
T	$0.948 \pm 0.003 \pm 0.004$	0.944	0.942	0.942	0.943
T_{major}	$0.149 \pm 0.006 \pm 0.006$	0.158	0.158	0.151	0.157
T_{minor}	$0.072 \pm 0.002 \pm 0.003$	0.073	0.076	0.085	0.076
O	$0.077 \pm 0.004 \pm 0.006$	0.085	0.082	0.067	0.081
S	$0.052 \pm 0.005 \pm 0.007$	0.060	0.062	0.055	0.061
A	$0.007 \pm 0.001 \pm 0.000$	0.007	0.008	0.009	0.008
C	$0.212 \pm 0.010 \pm 0.011$	0.225	0.227	0.233	0.226
M_H	$0.182 \pm 0.005 \pm 0.004$	0.190	0.193	0.195	0.191
B_T	$0.090 \pm 0.003 \pm 0.004$	0.095	0.095	0.095	0.095
B_W	$0.063 \pm 0.003 \pm 0.003$	0.068	0.067	0.066	0.066
D_2	$0.014 \pm 0.002 \pm 0.004$	0.019	0.019	0.016	0.019
	Width (σ)				
T	$0.048 \pm 0.003 \pm 0.008$	0.058	0.061	0.057	0.058
T_{major}	$0.099 \pm 0.005 \pm 0.012$	0.112	0.113	0.104	0.111
T_{minor}	$0.042 \pm 0.004 \pm 0.002$	0.041	0.045	0.044	0.043
O	$0.073 \pm 0.004 \pm 0.014$	0.088	0.086	0.076	0.086
S	$0.078 \pm 0.007 \pm 0.027$	0.099	0.104	0.093	0.101
A	$0.011 \pm 0.002 \pm 0.008$	0.014	0.016	0.015	0.015
C	$0.171 \pm 0.009 \pm 0.016$	0.185	0.189	0.182	0.185
M_H	$0.086 \pm 0.004 \pm 0.010$	0.096	0.096	0.090	0.093
B_T	$0.055 \pm 0.003 \pm 0.006$	0.061	0.062	0.058	0.061
B_W	$0.045 \pm 0.003 \pm 0.004$	0.050	0.050	0.046	0.049
D_2	$0.023 \pm 0.003 \pm 0.015$	0.038	0.039	0.034	0.038
	Skewness				
T	$-1.32 \pm 0.14 \pm 0.54$	-2.02	-2.08	-2.03	-2.06
T_{major}	$0.92 \pm 0.10 \pm 0.42$	1.35	1.42	1.50	1.39
T_{minor}	$1.78 \pm 0.36 \pm 0.10$	2.13	2.16	1.78	2.14
O	$0.98 \pm 0.10 \pm 1.30$	1.73	1.80	2.08	1.78
S	$2.69 \pm 0.29 \pm 2.50$	3.07	3.07	3.39	3.07
A	$-6.90 \pm 2.04 \pm 24.8$	8.68	7.00	6.33	7.23
C	$1.10 \pm 0.11 \pm 0.14$	1.30	1.35	1.29	1.34
M_H	$0.95 \pm 0.11 \pm 0.18$	1.19	1.20	1.07	1.23
B_T	$0.95 \pm 0.10 \pm 0.30$	1.28	1.35	1.36	1.32
B_W	$1.17 \pm 0.11 \pm 0.20$	1.39	1.44	1.45	1.45
D_2	$1.20 \pm 0.14 \pm 3.61$	3.46	3.54	3.92	3.58

Table 6: The mean, width and skewness of the event shape distributions compared to the PYTHIA, HERWIG, COJETS and ARIADNE Monte Carlo predictions.

y_{cut}	R_2	R_3	R_4	R_5
0.005	$20.1 \pm 2.2 \pm 0.6$	$49.4 \pm 2.9 \pm 1.5$	$25.5 \pm 2.5 \pm 1.3$	$5.0 \pm 1.5 \pm 1.6$
0.009	$31.1 \pm 2.6 \pm 0.6$	$47.0 \pm 2.9 \pm 1.5$	$19.3 \pm 2.4 \pm 1.3$	$1.5 \pm 1.1 \pm 1.6$
0.013	$39.8 \pm 2.7 \pm 0.8$	$45.9 \pm 2.9 \pm 1.2$	$12.8 \pm 2.1 \pm 1.2$	$1.5 \pm 1.0 \pm 1.0$
0.020	$50.7 \pm 2.8 \pm 1.3$	$42.1 \pm 2.9 \pm 1.0$	$6.6 \pm 1.7 \pm 1.5$	$0.6 \pm 0.6 \pm 1.0$
0.030	$62.7 \pm 2.7 \pm 2.1$	$34.4 \pm 2.8 \pm 2.0$	$3.0 \pm 1.4 \pm 1.5$	-
0.040	$69.6 \pm 2.7 \pm 1.8$	$29.5 \pm 2.7 \pm 2.0$	$0.8 \pm 1.1 \pm 0.9$	-
0.050	$74.7 \pm 2.6 \pm 1.3$	$25.0 \pm 2.6 \pm 1.9$	$0.3 \pm 0.8 \pm 0.9$	-
0.060	$78.7 \pm 2.4 \pm 0.9$	$21.3 \pm 2.5 \pm 1.4$	-	-
0.070	$81.7 \pm 2.3 \pm 0.9$	$18.7 \pm 2.4 \pm 1.1$	-	-
0.080	$85.5 \pm 2.1 \pm 1.4$	$14.5 \pm 2.2 \pm 1.7$	-	-
0.095	$89.4 \pm 1.9 \pm 1.4$	$10.6 \pm 2.0 \pm 1.9$	-	-
0.115	$92.9 \pm 1.6 \pm 1.3$	$7.0 \pm 1.7 \pm 2.1$	-	-
0.135	$95.0 \pm 1.4 \pm 0.9$	$5.0 \pm 1.4 \pm 1.4$	-	-
0.160	$97.1 \pm 1.1 \pm 0.4$	$2.9 \pm 1.2 \pm 0.7$	-	-
0.188	$99.0 \pm 0.8 \pm 0.4$	$1.0 \pm 0.8 \pm 0.7$	-	-

Table 7: Measured values for jet production rates, in percent, using the JADE (E0) scheme. The first error is statistical, the second systematic.

y_{cut}	R_2	R_3	R_4	R_5
0.0008	$19.2 \pm 2.3 \pm 3.5$	$37.8 \pm 2.8 \pm 2.1$	$24.4 \pm 2.4 \pm 4.3$	$18.7 \pm 2.2 \pm 2.5$
0.0013	$30.2 \pm 2.6 \pm 3.5$	$40.7 \pm 2.8 \pm 2.1$	$20.8 \pm 2.3 \pm 4.3$	$8.4 \pm 1.8 \pm 2.5$
0.0023	$45.6 \pm 2.8 \pm 3.4$	$35.5 \pm 2.7 \pm 1.0$	$14.6 \pm 2.1 \pm 2.3$	$4.2 \pm 1.4 \pm 1.8$
0.0040	$54.3 \pm 2.8 \pm 3.4$	$33.5 \pm 2.7 \pm 0.6$	$10.1 \pm 1.9 \pm 0.4$	$2.0 \pm 1.0 \pm 1.8$
0.0070	$63.5 \pm 2.8 \pm 2.3$	$28.9 \pm 2.6 \pm 0.8$	$7.8 \pm 1.8 \pm 1.1$	-
0.012	$71.6 \pm 2.6 \pm 2.0$	$23.7 \pm 2.5 \pm 0.9$	$5.1 \pm 1.7 \pm 1.1$	-
0.023	$79.7 \pm 2.4 \pm 1.4$	$19.4 \pm 2.4 \pm 1.1$	$1.0 \pm 1.1 \pm 1.1$	-
0.04	$88.2 \pm 2.0 \pm 1.6$	$11.9 \pm 2.0 \pm 1.7$	-	-
0.07	$95.3 \pm 1.5 \pm 1.6$	$4.5 \pm 1.5 \pm 1.7$	-	-
0.13	$99.2 \pm 0.8 \pm 1.4$	$0.9 \pm 0.8 \pm 1.7$	-	-
0.24	$100.0 \pm 0.0 \pm 1.4$	-	-	-

Table 8: Measured values for jet production rates, in percent, using the Durham (D) scheme. The first error is statistical, the second systematic.

R [rad]	R_2	R_3	R_4
0.3	$52.5 \pm 2.9 \pm 2.4$	$29.3 \pm 2.6 \pm 1.2$	$18.2 \pm 2.3 \pm 1.5$
0.5	$61.6 \pm 2.8 \pm 2.4$	$27.8 \pm 2.6 \pm 1.2$	$10.6 \pm 2.0 \pm 1.5$
0.7	$70.3 \pm 2.6 \pm 1.9$	$24.8 \pm 2.5 \pm 1.0$	$4.8 \pm 1.5 \pm 1.3$
0.9	$77.6 \pm 2.4 \pm 1.5$	$21.1 \pm 2.4 \pm 0.8$	$1.2 \pm 0.9 \pm 1.3$
1.1	$87.9 \pm 1.9 \pm 0.8$	$12.1 \pm 2.0 \pm 1.0$	-
1.3	$95.9 \pm 1.2 \pm 1.0$	$3.9 \pm 1.4 \pm 1.2$	-
1.5	$99.6 \pm 0.7 \pm 1.0$	$0.4 \pm 0.7 \pm 1.2$	-

Table 9: Measured values of jet production rates, in percent, using the cone jet finder with fixed $\varepsilon = 7$ GeV and variable R. The first error is statistical, the second systematic.

ε [GeV]	R_2	R_3	R_4
2	$49.8 \pm 2.9 \pm 2.6$	$33.2 \pm 2.6 \pm 1.3$	$17.2 \pm 2.4 \pm 2.2$
6	$68.0 \pm 2.7 \pm 2.6$	$26.2 \pm 2.6 \pm 1.3$	$5.8 \pm 1.6 \pm 2.2$
10	$76.2 \pm 2.5 \pm 3.4$	$21.7 \pm 2.4 \pm 2.2$	$1.9 \pm 1.2 \pm 0.9$
14	$81.2 \pm 2.3 \pm 3.3$	$17.6 \pm 2.3 \pm 2.5$	$1.1 \pm 1.0 \pm 0.5$
18	$82.6 \pm 2.3 \pm 2.5$	$16.7 \pm 2.2 \pm 1.8$	$0.7 \pm 0.9 \pm 0.5$
22	$86.6 \pm 2.1 \pm 1.9$	$13.4 \pm 2.1 \pm 1.4$	-
25.5	$89.4 \pm 2.0 \pm 1.9$	$10.6 \pm 1.9 \pm 1.4$	-

Table 10: Measured values of jet production rates, in percent, using the cone jet finder with fixed $R = 0.7$ and variable ε. The first error is statistical, the second systematic.

D_2	$1/\sigma \cdot \mathrm{d}\sigma/\mathrm{d}D_2$
0.0003 – 0.0008	$337. \pm 54. \pm 21.$
0.0008 – 0.0013	$201. \pm 36. \pm 21.$
0.0013 – 0.0023	$154. \pm 23. \pm 20.$
0.0023 – 0.0040	$51. \pm 10. \pm 20.$
0.0040 – 0.0070	$30.5 \pm 6.0 \pm 2.8$
0.0070 – 0.0120	$16.2 \pm 3.4 \pm 2.6$
0.0120 – 0.0225	$7.6 \pm 1.7 \pm 2.2$
0.0225 – 0.0400	$4.9 \pm 1.1 \pm 1.5$
0.0400 – 0.0700	$2.38 \pm 0.58 \pm 0.58$
0.0700 – 0.1300	$0.62 \pm 0.25 \pm 0.27$
0.1300 – 0.2350	$0.08 \pm 0.08 \pm 0.27$

Table 11: Measured values for the D_2 distribution measured with the Durham jet finding algorithm. The first error is statistical, the second systematic.

	$1-T$	M_H	B_T	B_W	D_2
α_s(161 GeV)	**0.1057**	**0.1043**	**0.1021**	**0.0909**	**0.1020**
fit range	$0.05-0.3$	$0.17-0.45$	$0.075-0.25$	$0.05-0.2$	$0.0023-0.130$
χ^2/d.o.f.	6.9/5	4.3/4	7.9/5	13/4	3.6/6
Statistical error	±0.0068	±0.0068	±0.0053	±0.0045	±0.0054
tracks only	<0.0001	<0.0001	$+0.0089$	$+0.0087$	$+0.0065$
cluster only	<0.0001	<0.0001	<0.0001	$+0.0036$	<0.0001
energy balance	$+0.0045$	$+0.0022$	<0.0001	$+0.0027$	<0.0001
M_{W}^{fit}	-0.0048	-0.0069	<0.0001	-0.0008	-0.0010
Experimental syst.	±0.0066	±0.0073	±0.0089	±0.0091	±0.0066
$b+1$ s.d.	$+0.0001$	$+0.0002$	$+0.0002$	<0.0001	-0.0001
$b-1$ s.d.	-0.0001	-0.0002	-0.0003	-0.0001	$+0.0001$
σ_q+1 s.d.	-0.0002	<0.0001	-0.0003	-0.0002	<0.0001
σ_q-1 s.d.	$+0.0003$	$+0.0001$	$+0.0003$	$+0.0001$	-0.0001
$Q_0=4$ GeV	-0.0004	$+0.0009$	-0.0011	$+0.0004$	$+0.0016$
udsc only	$+0.0008$	<0.0001	$+0.0017$	$+0.0011$	$+0.0015$
HERWIG 5.9	-0.0007	-0.0001	-0.0023	-0.0003	-0.0010
ARIADNE 4.08	$+0.0015$	$+0.0010$	$+0.0004$	$+0.0010$	$+0.0009$
Total hadronisation	±0.0020	±0.0014	±0.0031	±0.0016	±0.0026
$x_\mu=0.5$	-0.0037	-0.0027	-0.0043	-0.0022	-0.0009
$x_\mu=2$	$+0.0047$	$+0.0038$	$+0.0051$	$+0.0029$	$+0.0025$
Total error	$\pm$**0.0106**	$\pm$**0.0105**	$\pm$**0.0118**	$\pm$**0.0106**	$\pm$**0.0091**

Table 12: Values of α_s(161 GeV) derived using the $\mathcal{O}(\alpha_s^2)$+NLLA QCD calculations with $x_\mu=1$ and the $\ln(R)$-matching scheme, fit ranges and χ^2/d.o.f. values for each of the five event shape observables. In addition, the statistical and systematic uncertainties are given. Where a signed value is quoted, this indicates the direction in which α_s(161 GeV) changed with respect to the standard analysis. The scale uncertainty is treated as an asymmetrical uncertainty on α_s.

$p_\perp^{\rm in}$	$1/\sigma \cdot {\rm d}\sigma_{\rm ch}/{\rm d}p_\perp^{\rm in}$
0.0 – 0.1	51.7 ± 1.4 ± 0.9
0.1 – 0.2	39.4 ± 1.2 ± 0.9
0.2 – 0.3	31.1 ± 1.1 ± 1.0
0.3 – 0.4	23.6 ± 1.0 ± 0.6
0.4 – 0.5	15.2 ± 0.8 ± 0.5
0.5 – 0.6	12.5 ± 0.7 ± 0.5
0.6 – 0.7	10.9 ± 0.6 ± 0.4
0.7 – 0.8	7.93 ± 0.55 ± 0.33
0.8 – 0.9	6.82 ± 0.52 ± 0.11
0.9 – 1.0	5.10 ± 0.45 ± 0.10
1.0 – 1.2	4.20 ± 0.29 ± 0.16
1.2 – 1.4	3.09 ± 0.25 ± 0.12
1.4 – 1.6	2.27 ± 0.21 ± 0.20
1.6 – 2.0	1.45 ± 0.12 ± 0.14
2.0 – 2.5	0.93 ± 0.09 ± 0.12
2.3 – 3.0	0.61 ± 0.07 ± 0.05
3.0 – 3.5	0.48 ± 0.06 ± 0.06
3.5 – 4.0	0.12 ± 0.03 ± 0.05
4.0 – 5.0	0.15 ± 0.02 ± 0.04
5.0 – 6.0	0.06 ± 0.02 ± 0.02
6.0 – 7.0	0.02 ± 0.01 ± 0.02
$\langle p_\perp^{\rm in}\rangle$	0.567 ± 0.011 ± 0.034

$p_\perp^{\rm out}$	$1/\sigma \cdot {\rm d}\sigma_{\rm ch}/{\rm d}p_\perp^{\rm out}$
0.0 – 0.1	72.3 ± 1.7 ± 2.1
0.1 – 0.2	58.0 ± 1.5 ± 2.1
0.2 – 0.3	38.6 ± 1.2 ± 1.7
0.3 – 0.4	25.4 ± 1.0 ± 1.8
0.4 – 0.5	16.4 ± 0.8 ± 1.4
0.5 – 0.6	11.0 ± 0.7 ± 1.2
0.6 – 0.7	5.95 ± 0.48 ± 1.02
0.7 – 0.8	4.22 ± 0.41 ± 0.90
0.8 – 0.9	2.70 ± 0.33 ± 0.74
0.9 – 1.0	2.06 ± 0.28 ± 0.64
1.0 – 1.2	0.96 ± 0.14 ± 0.51
1.2 – 1.4	0.84 ± 0.13 ± 0.37
1.4 – 1.6	0.41 ± 0.09 ± 0.27
1.6 – 2.0	0.14 ± 0.04 ± 0.19
2.0 – 2.4	0.08 ± 0.03 ± 0.12
2.4 – 2.8	0.05 ± 0.02 ± 0.07
2.8 – 3.2	0.02 ± 0.01 ± 0.04
3.2 – 3.6	0.02 ± 0.01 ± 0.03
3.6 – 4.0	0.02 ± 0.01 ± 0.03
$\langle p_\perp^{\rm out}\rangle$	0.260 ± 0.004 ± 0.004

Table 13: Measured values of the momentum spectra in, $p_\perp^{\rm in}$, and out, $p_\perp^{\rm out}$, of the event plane. The first error is statistical, the second systematic. The mean values are also shown.

y	$1/\sigma \cdot \mathrm{d}\sigma_{\mathrm{ch}}/\mathrm{d}y$
0.0 – 0.5	6.70 ± 0.26 ± 0.42
0.5 – 1.0	6.71 ± 0.25 ± 0.42
1.0 – 1.5	7.39 ± 0.24 ± 0.29
1.5 – 2.0	6.99 ± 0.23 ± 0.16
2.0 – 2.5	6.70 ± 0.22 ± 0.13
2.5 – 3.0	5.22 ± 0.19 ± 0.17
3.0 – 3.5	4.41 ± 0.18 ± 0.16
3.5 – 4.0	2.41 ± 0.13 ± 0.11
4.0 – 4.5	1.30 ± 0.10 ± 0.08
4.5 – 5.0	0.42 ± 0.06 ± 0.05
5.0 – 5.5	0.09 ± 0.03 ± 0.03
5.5 – 6.0	0.01 ± 0.01 ± 0.01
6.0 – 6.5	0.01 ± 0.01 ± 0.01
$\langle y \rangle$	1.836 ± 0.013 ± 0.023

Table 14: Measured values for the Rapidity y distribution. The first error is statistical, the second systematic. The mean value is also shown.

x_p	$1/\sigma \cdot \mathrm{d}\sigma_{\mathrm{ch}}/\mathrm{d}x_p$	x_p	$1/\sigma \cdot \mathrm{d}\sigma_{\mathrm{ch}}/\mathrm{d}x_p$
0.00 – 0.01	712 ± 17 ± 10	0.12 – 0.14	25.6 ± 2.3 ± 0.5
0.01 – 0.02	444 ± 13 ± 10	0.14 – 0.16	20.5 ± 2.0 ± 0.5
0.02 – 0.03	267 ± 10 ± 6.2	0.16 – 0.18	17.1 ± 1.9 ± 0.5
0.03 – 0.04	187 ± 8.4 ± 7.9	0.18 – 0.20	13.4 ± 1.7 ± 0.5
0.04 – 0.05	125 ± 6.9 ± 5.4	0.20 – 0.25	8.4 ± 0.8 ± 0.4
0.05 – 0.06	103 ± 6.3 ± 6.5	0.25 – 0.30	4.2 ± 0.6 ± 0.3
0.06 – 0.07	81.6 ± 5.6 ± 4.4	0.30 – 0.40	2.6 ± 0.3 ± 0.2
0.07 – 0.08	63.9 ± 5.0 ± 3.9	0.40 – 0.50	1.1 ± 0.2 ± 0.1
0.08 – 0.09	59.4 ± 4.8 ± 3.4	0.50 – 0.60	0.4 ± 0.1 ± 0.03
0.09 – 0.10	47.0 ± 4.3 ± 1.6	0.60 – 0.80	0.10 ± 0.04 ± 0.03
0.10 - 0.12	37.8 ± 2.7 ± 1.2	$\langle x_p \rangle$	0.0486 ± 0.0009 ± 0.0001

Table 15: Measured values for the fragmentation function x_p. The first error is statistical, the second systematic. The mean value is also shown.

ξ_p	$1/\sigma \cdot \mathrm{d}\sigma_{\mathrm{ch}}/\mathrm{d}\xi_p$	ξ_p	$1/\sigma \cdot \mathrm{d}\sigma_{\mathrm{ch}}/\mathrm{d}\xi_p$
0.0 – 0.2	0.01 ± 0.01 ± 0.02	3.2 – 3.4	6.31 ± 0.35 ± 0.29
0.2 – 0.4	0.06 ± 0.03 ± 0.02	3.4 – 3.6	6.75 ± 0.36 ± 0.21
0.4 – 0.6	0.12 ± 0.04 ± 0.02	3.6 – 3.8	6.60 ± 0.35 ± 0.25
0.6 – 0.8	0.37 ± 0.08 ± 0.04	3.8 – 4.0	6.50 ± 0.35 ± 0.22
0.8 – 1.0	0.51 ± 0.10 ± 0.07	4.0 – 4.2	6.70 ± 0.36 ± 0.18
1.0 – 1.2	1.05 ± 0.15 ± 0.09	4.2 – 4.4	6.24 ± 0.34 ± 0.15
1.2 – 1.4	1.24 ± 0.16 ± 0.10	4.4 – 4.6	6.35 ± 0.35 ± 0.20
1.4 – 1.6	1.88 ± 0.20 ± 0.10	4.6 – 4.8	6.43 ± 0.34 ± 0.27
1.6 – 1.8	2.60 ± 0.23 ± 0.11	4.8 – 5.0	5.86 ± 0.33 ± 0.30
1.8 – 2.0	3.20 ± 0.25 ± 0.11	5.0 – 5.2	4.81 ± 0.30 ± 0.23
2.0 – 2.2	3.44 ± 0.26 ± 0.09	5.2 – 5.4	4.38 ± 0.28 ± 0.14
2.2 – 2.4	4.37 ± 0.29 ± 0.10	5.4 – 5.6	3.90 ± 0.27 ± 0.07
2.4 – 2.6	4.95 ± 0.31 ± 0.20	5.6 – 5.8	2.67 ± 0.23 ± 0.12
2.6 – 2.8	5.28 ± 0.32 ± 0.24	5.8 – 6.0	2.65 ± 0.24 ± 0.16
2.8 – 3.0	5.45 ± 0.32 ± 0.34	6.0 – 6.2	1.83 ± 0.22 ± 0.19
3.0 – 3.2	5.54 ± 0.32 ± 0.28	6.2 – 6.4	0.60 ± 0.27 ± 0.19

Table 16: Measured values for the ξ_p distribution. The first error is statistical, the second systematic.

	ξ_0	$\langle n_{\mathrm{ch}}\rangle$		D	$\langle n_{\mathrm{ch}}\rangle/D$	C_2	$\mathcal{R}_2$
		frag.	mult.				
standard result	4.00	24.25	24.46	7.68	3.19	1.099	1.058
statistical error	0.03	0.43	0.45	0.37	0.14	0.009	0.009
energy balance	<0.01	−0.52	−0.33	<0.01	<0.01	<0.001	<0.001
$\lvert d_0\rvert < 5$ cm	<0.01	+0.03	+0.18	+0.10	−0.02	+0.001	+0.001
$\lvert\cos\theta_T\rvert < 0.7$	−0.01	<0.01	<0.01	<0.01	<0.01	<0.001	<0.001
M_{W}^{fit}	+0.02	<0.01	−0.18	<0.01	<0.01	<0.001	<0.001
HERWIG 5.8d	−0.01	−0.16	−0.04	−0.28	0.11	−0.007	−0.007
EXCALIBUR	<0.01	−0.04	−0.13	−0.06	0.01	<0.001	−0.001
Tot. syst. error	0.02	0.55	0.44	0.30	0.11	0.007	0.007

Table 17: Results with statistical and systematic uncertainties for the position ξ_0 of the peak of the ξ_p distribution, for $\langle n_{\mathrm{ch}}\rangle$ based upon measurements of the multiplicity distribution (mult.) or the fragmentation function (frag.), the dispersion D, the ratio $\langle n_{\mathrm{ch}}\rangle/D$ and the second moments C_2 and $\mathcal{R}_2$. The signs indicate the direction of the changes with respect to the standard analysis.

n_{ch}	$P(n_{ch})$ [%]	n_{ch}	$P(n_{ch})$ [%]
8	$0.24 \pm 0.11 \pm 0.24$	34	$4.13 \pm 0.50 \pm 0.43$
10	$1.10 \pm 0.29 \pm 0.24$	36	$3.54 \pm 0.50 \pm 0.35$
12	$2.64 \pm 0.49 \pm 0.56$	38	$2.29 \pm 0.36 \pm 0.29$
14	$4.79 \pm 0.64 \pm 0.98$	40	$1.45 \pm 0.27 \pm 0.21$
16	$7.39 \pm 0.81 \pm 1.05$	42	$0.89 \pm 0.19 \pm 0.18$
18	$9.56 \pm 0.91 \pm 0.77$	44	$0.55 \pm 0.14 \pm 0.11$
20	$10.3 \pm 0.9 \pm 0.5$	46	$0.35 \pm 0.13 \pm 0.07$
22	$10.9 \pm 0.9 \pm 0.5$	48	$0.27 \pm 0.13 \pm 0.08$
24	$10.5 \pm 0.9 \pm 0.6$	50	$0.16 \pm 0.09 \pm 0.08$
26	$9.33 \pm 0.81 \pm 0.60$	52	$0.14 \pm 0.11 \pm 0.09$
28	$7.65 \pm 0.70 \pm 0.60$	54	$0.10 \pm 0.09 \pm 0.05$
30	$6.44 \pm 0.65 \pm 0.56$	56	$0.08 \pm 0.08 \pm 0.05$
32	$5.17 \pm 0.56 \pm 0.47$		

Table 18: Charged particle multiplicity distribution in percent. The first error is statistical, the second systematic.

Figures

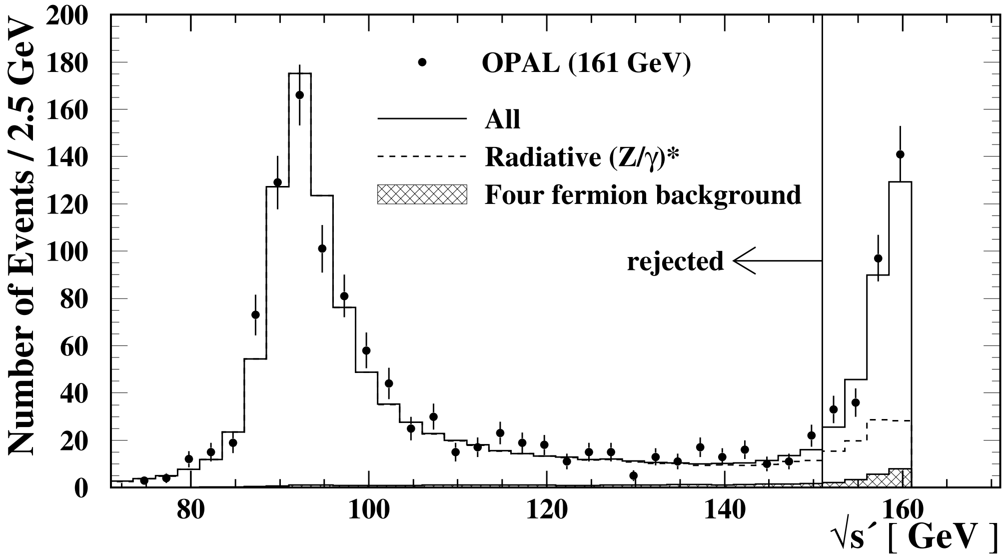

Figure 1: Distribution of reconstructed $\sqrt{s'}$ for the data (full points) with statistical errors. The PYTHIA predictions for all $(Z^0/\gamma)^*$ events (solid line) and for the radiative background (dashed line) are also shown. The hatched area indicates the 4-fermion background predicted by the grc4f Monte Carlo.

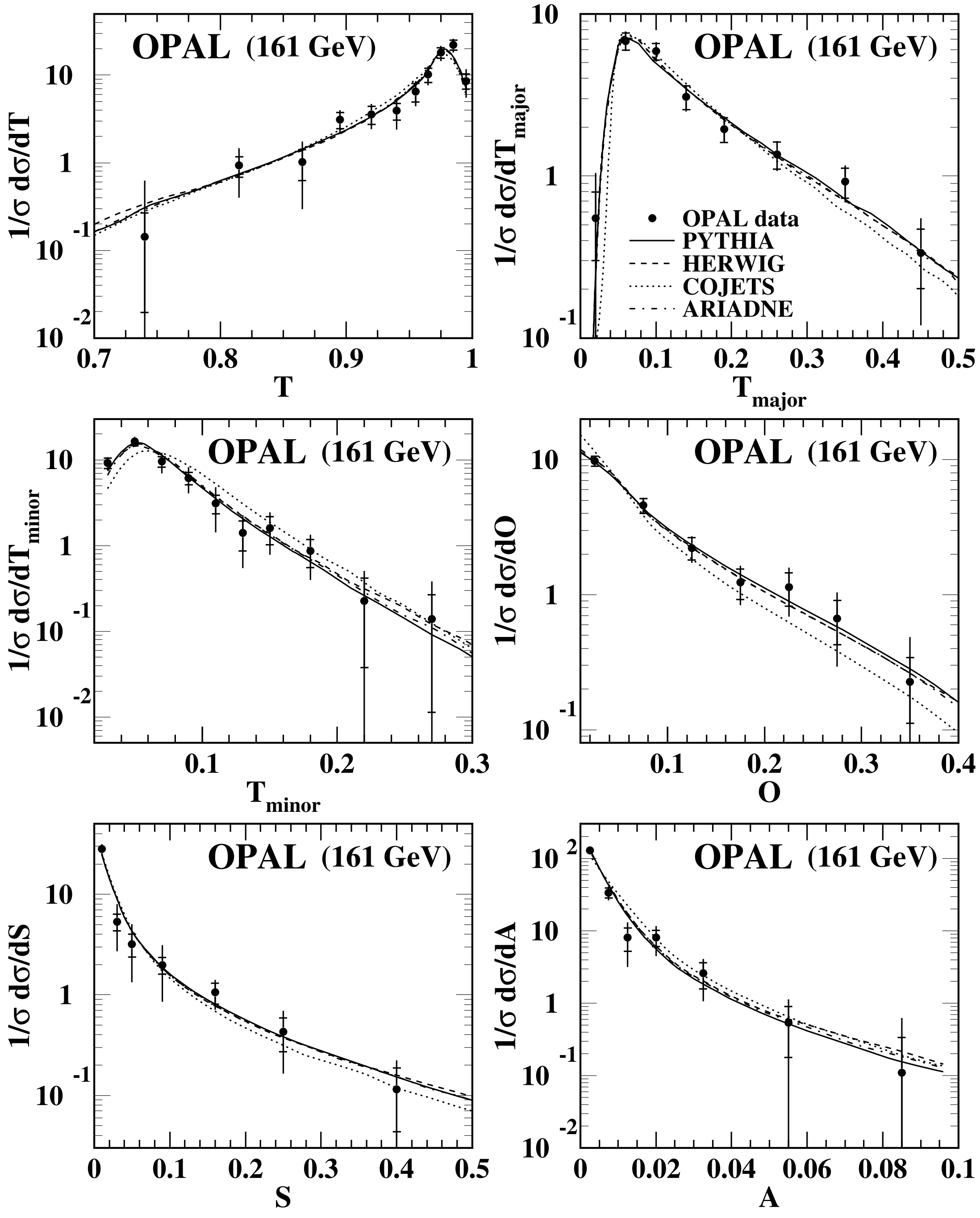

Figure 2: Distributions of the event shape observables Thrust T, Thrust Major T_{major} Thrust Minor T_{minor}, Oblateness O, Sphericity S and Aplanarity A. Experimental statistical errors are delimited by the small horizontal bars. The total errors are shown by the vertical error lines. Hadron level predictions from PYTHIA, HERWIG, COJETS and ARIADNE are also shown.

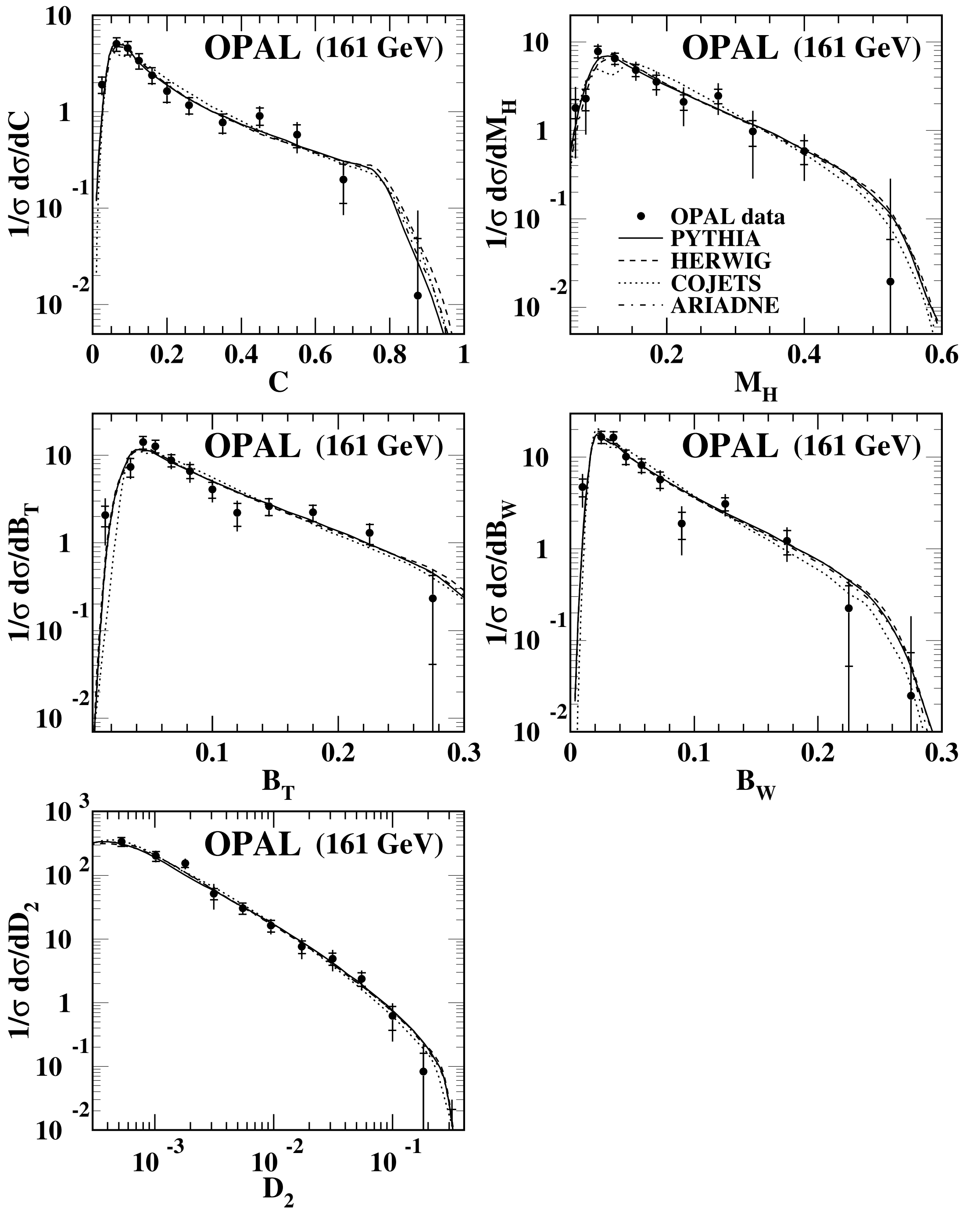

Figure 3: Distributions of the event shape observables C-parameter C, Heavy Jet Mass M_H, Total Jet Broadening B_T, Wide Jet Broadening B_W, and the Differential 2-jet rate D_2 using the Durham scheme. Experimental statistical errors are delimited by the small horizontal bars. The total errors are shown by the vertical error lines. Hadron level predictions from PYTHIA, HERWIG, COJETS and ARIADNE are also shown.

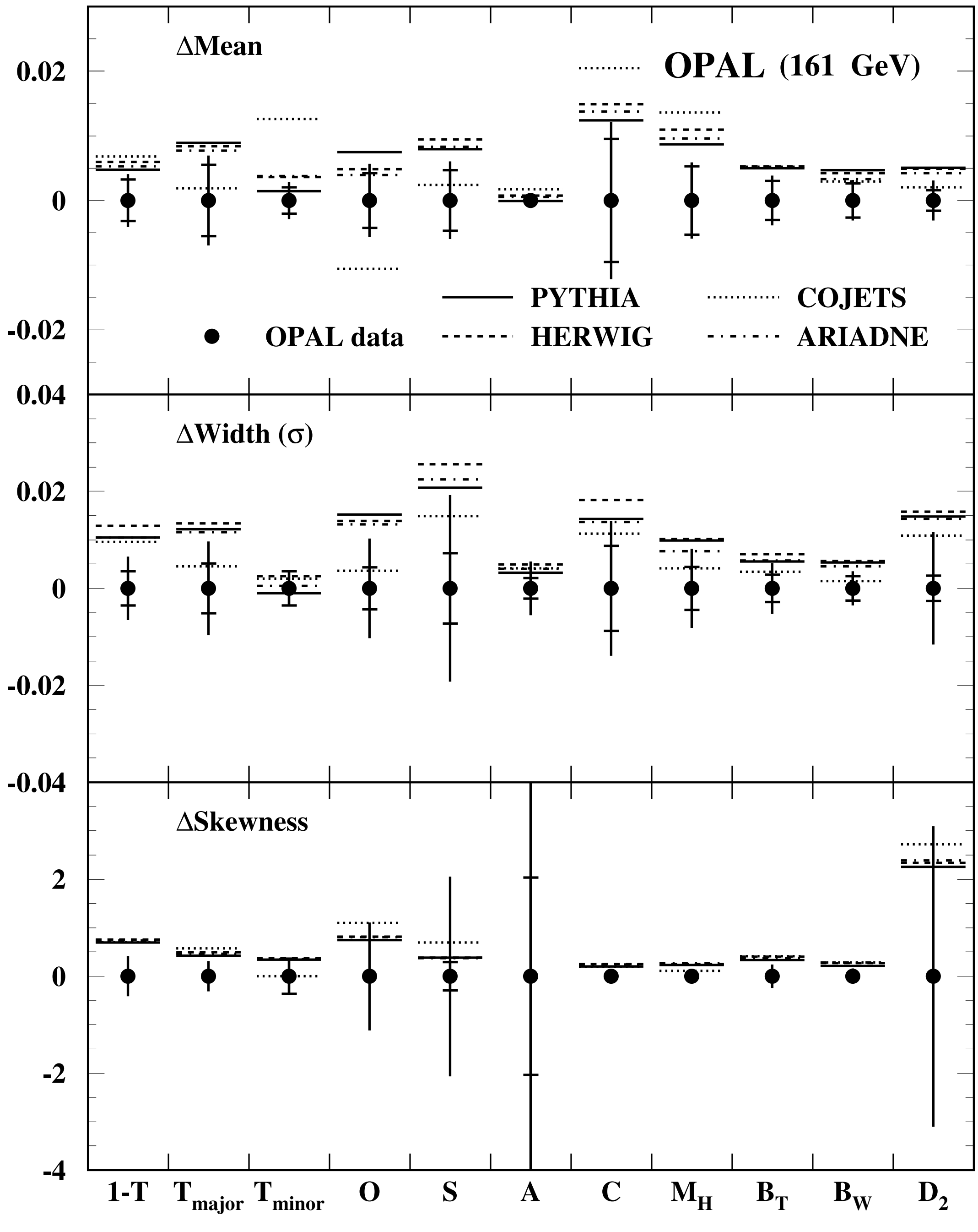

Figure 4: Difference of the PYTHIA, HERWIG, COJETS and ARIADNE predictions relative to the data (shown as full points with error bars) for the mean, width and skewness of event shape distributions. The Monte Carlo predictions for the skewness of the A distribution are off the scale of the figure.

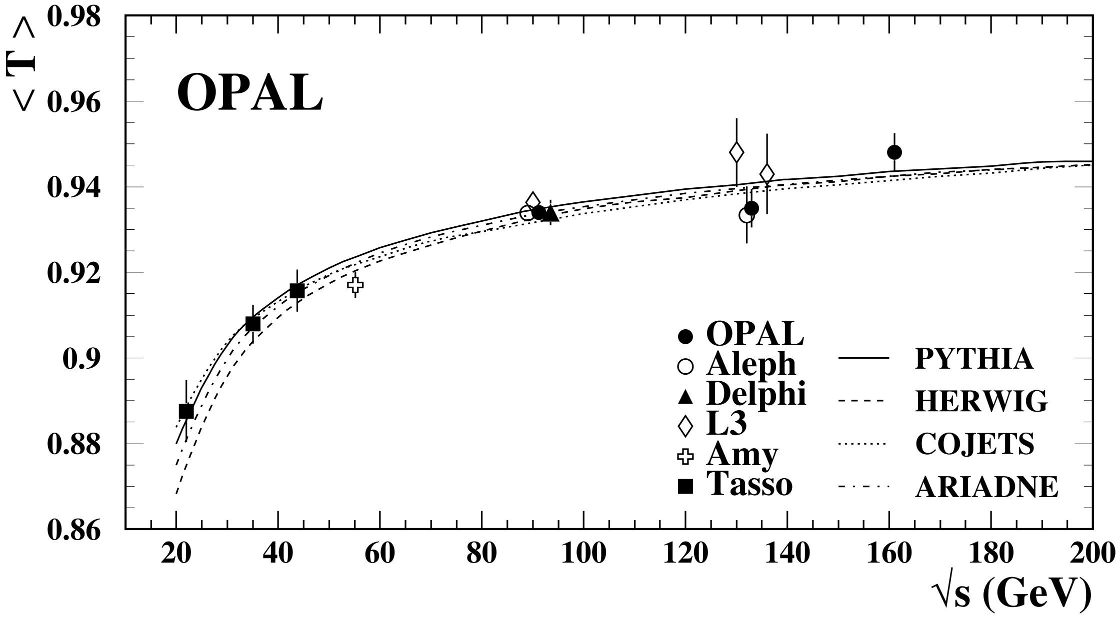

Figure 5: The mean Thrust value as a function of $\sqrt{s}$ from 22 GeV to 161 GeV. The measurements are compared to the predictions of PYTHIA, HERWIG, ARIADNE and COJETS.

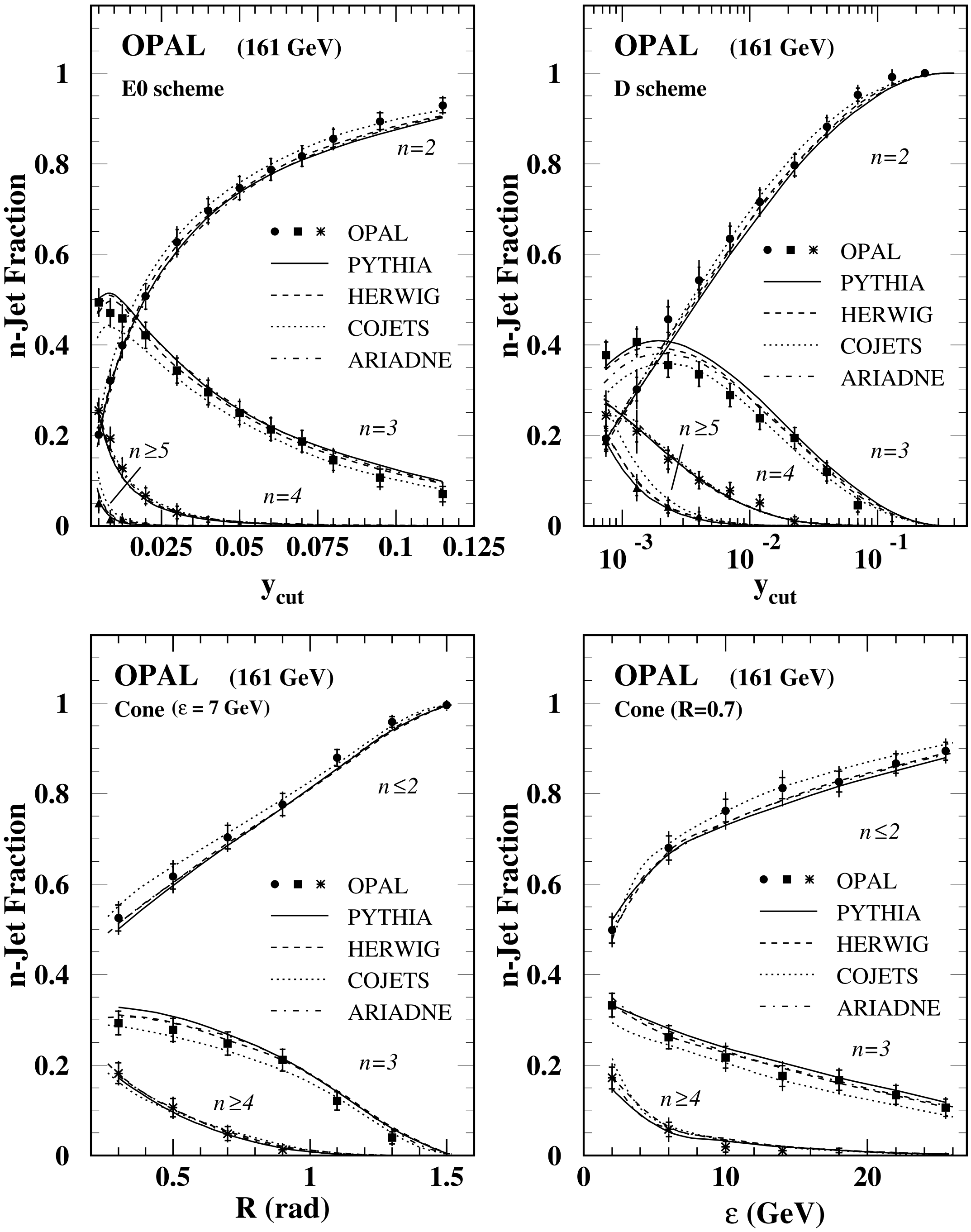

Figure 6: The fraction of the 2-, 3-, 4- and 5- or more jet events as a function of $y_{\rm cut}$ for the JADE (E0) and Durham (D) jet finding schemes, and the fraction of 2-, 3- and 4- or more jet events as a function of the energy cutoff ε or the cone half angle R for the cone jet finder. Hadron level predictions from PYTHIA, HERWIG, COJETS and ARIADNE are also shown.

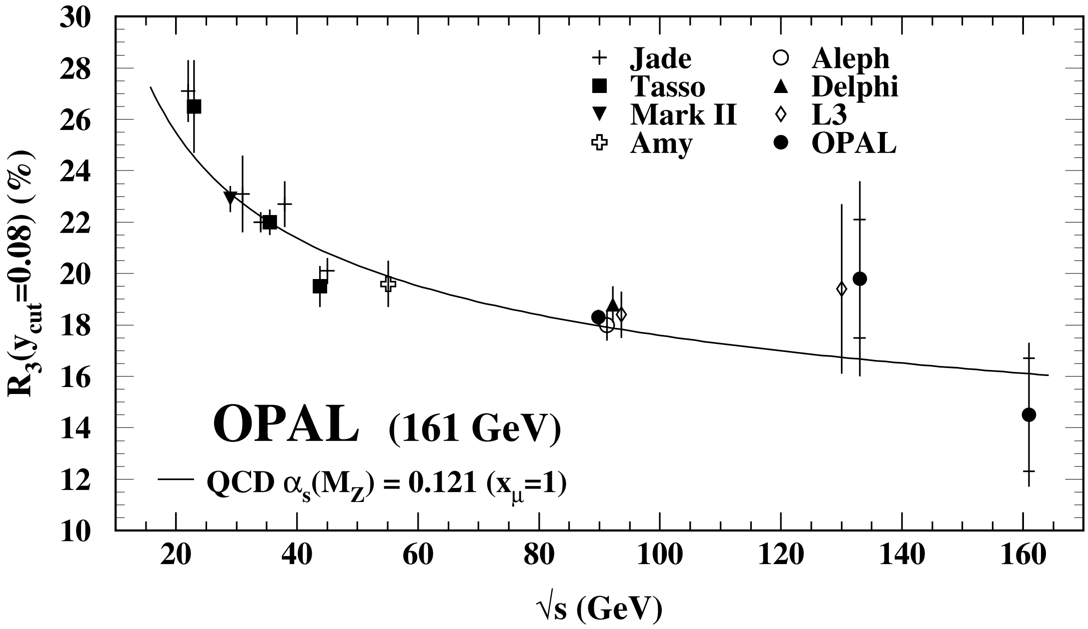

Figure 7: The three-jet rate (R_3) at $y_{\mathrm{cut}} = 0.08$ for the JADE (E0) jet finder, for values of $\sqrt{s}$ between 22 GeV and 161 GeV. The result of a fit of the $\mathcal{O}(\alpha_s^2)$ QCD prediction to the data is also shown.

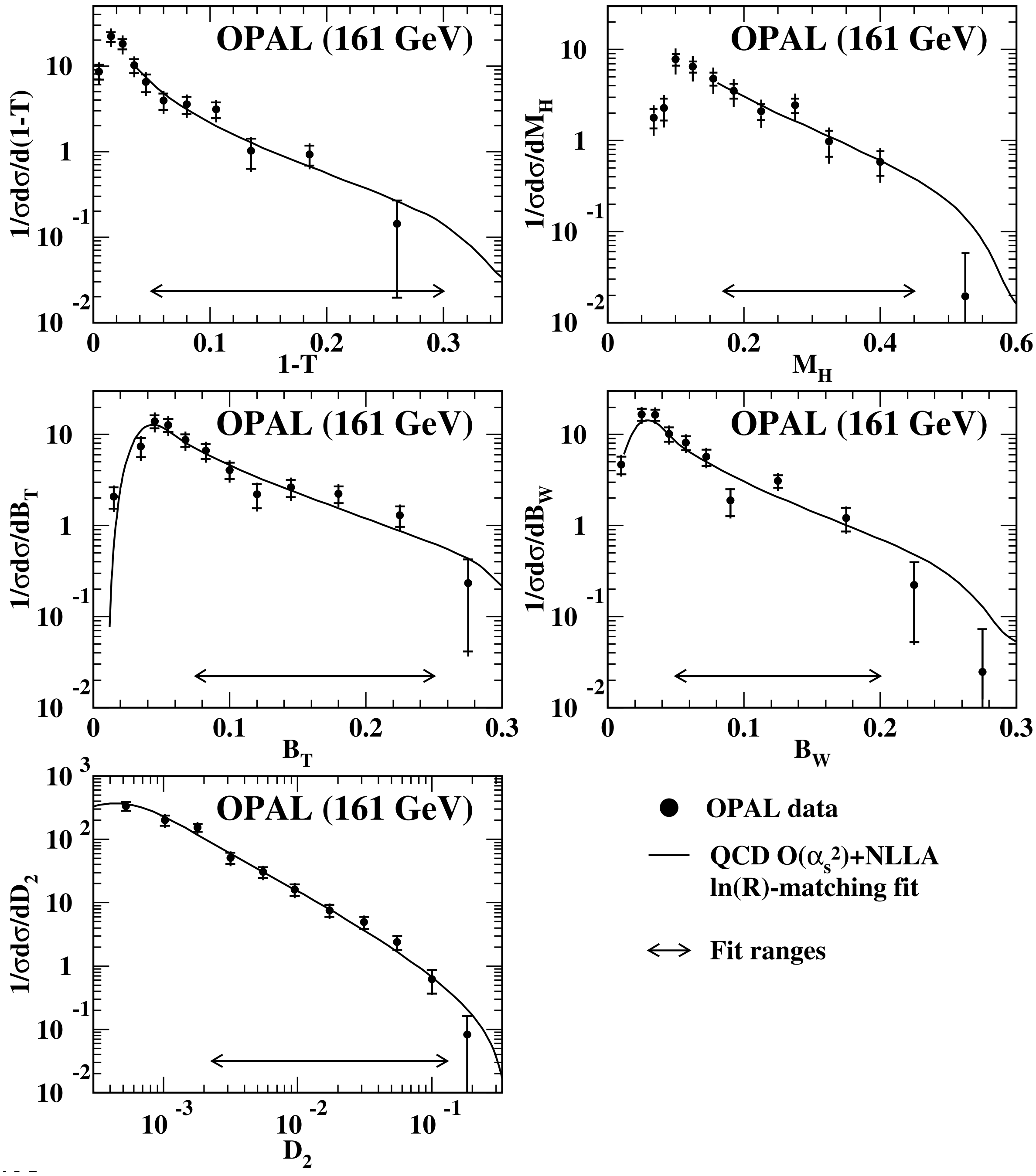

Figure 8: Distributions of the event shape observables Thrust $1-T$, Heavy Jet Mass M_H, Total B_T and Wide B_W Jet Broadening, and the Differential 2-jet rate D_2 using the Durham scheme are shown together with fits of the $\mathcal{O}(\alpha_s^2)$+NLLA QCD predictions. The fitted regions are indicated by the arrows.

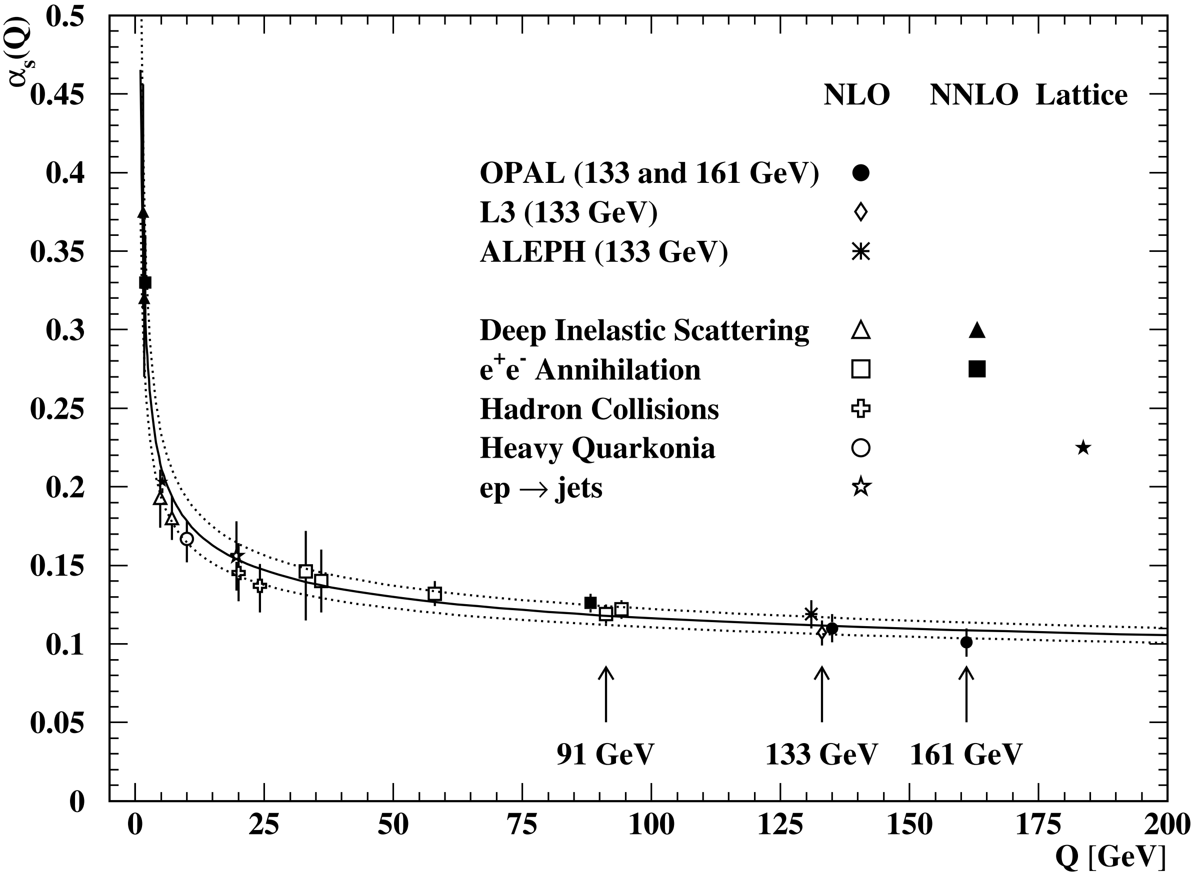

Figure 9: Values of α_s as function of energy [28]. The labels NLO and NNLO refer to the order of calculation used. NLO corresponds to $\mathcal{O}(\alpha_s^2)$ in e^+e^- annihilations, and NNLO to $\mathcal{O}(\alpha_s^3)$. The label Lattice refers to α_s values determined from lattice QCD calculations. The curves show the $\mathcal{O}(\alpha_s^3)$ QCD prediction for $\alpha_s(Q)$ using $\alpha_s(M_{Z^0}) = 0.118 \pm 0.006$; the full line shows the central value while the dotted lines indicate the variation given by the uncertainty.

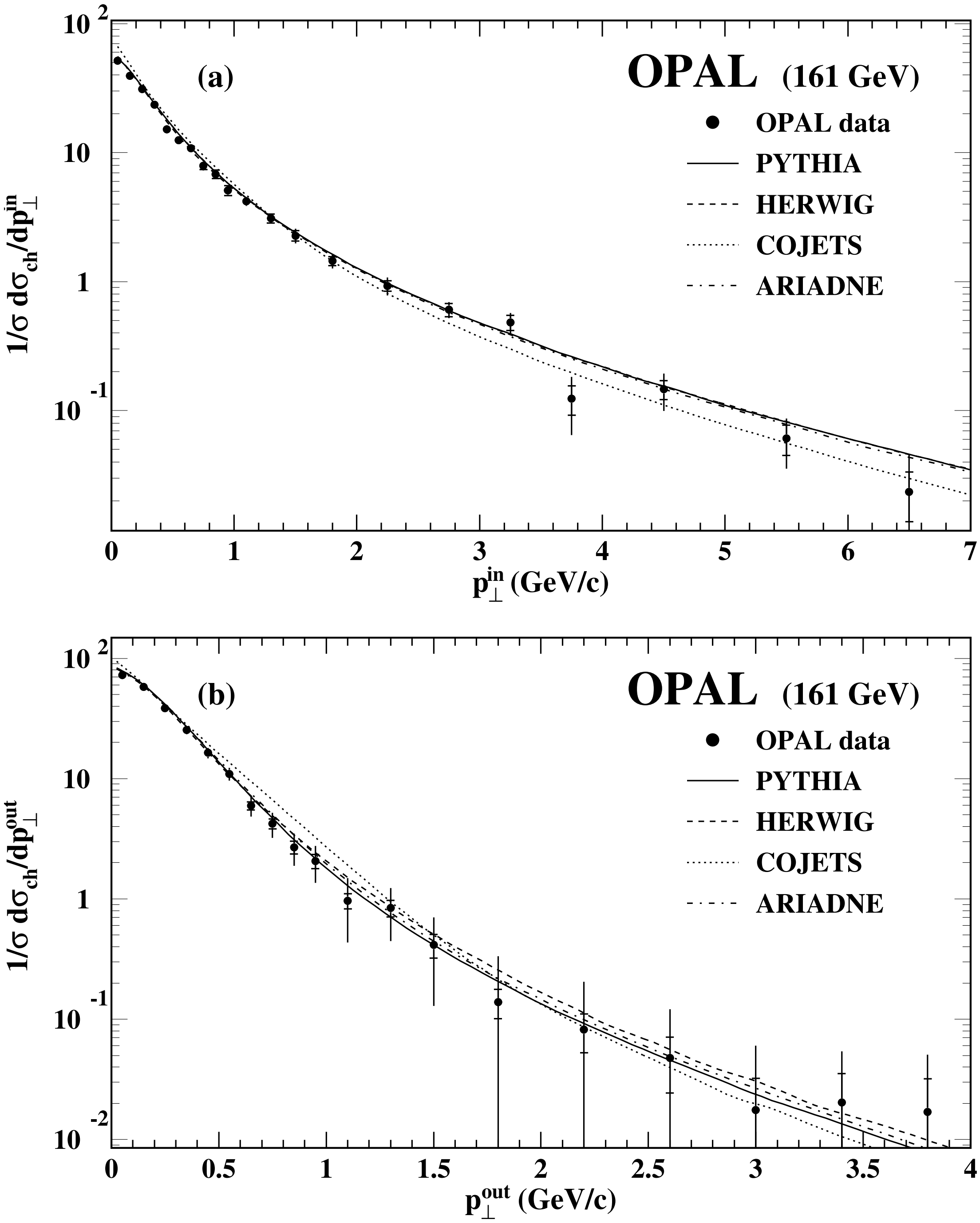

Figure 10: Distributions of momentum spectra in, $p_{\perp}^{\rm in}$, and out, $p_{\perp}^{\rm out}$, of the event plane for charged particles, compared to PYTHIA, HERWIG, COJETS and ARIADNE.

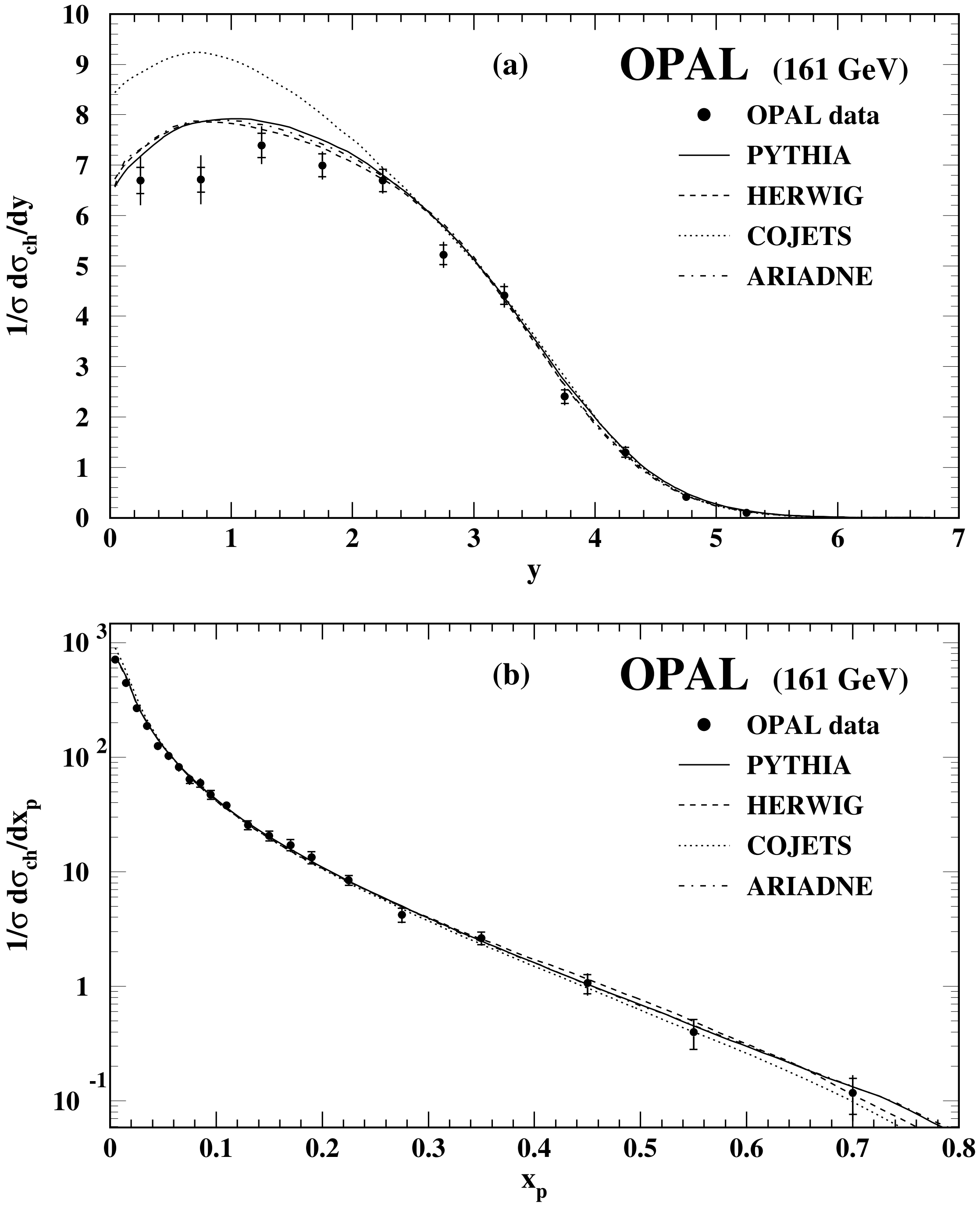

Figure 11: Distribution of Rapidity, y, and the fragmentation function, $x_p = 2p/\sqrt{s}$, for charged particles, compared to PYTHIA, HERWIG, COJETS and ARIADNE predictions.

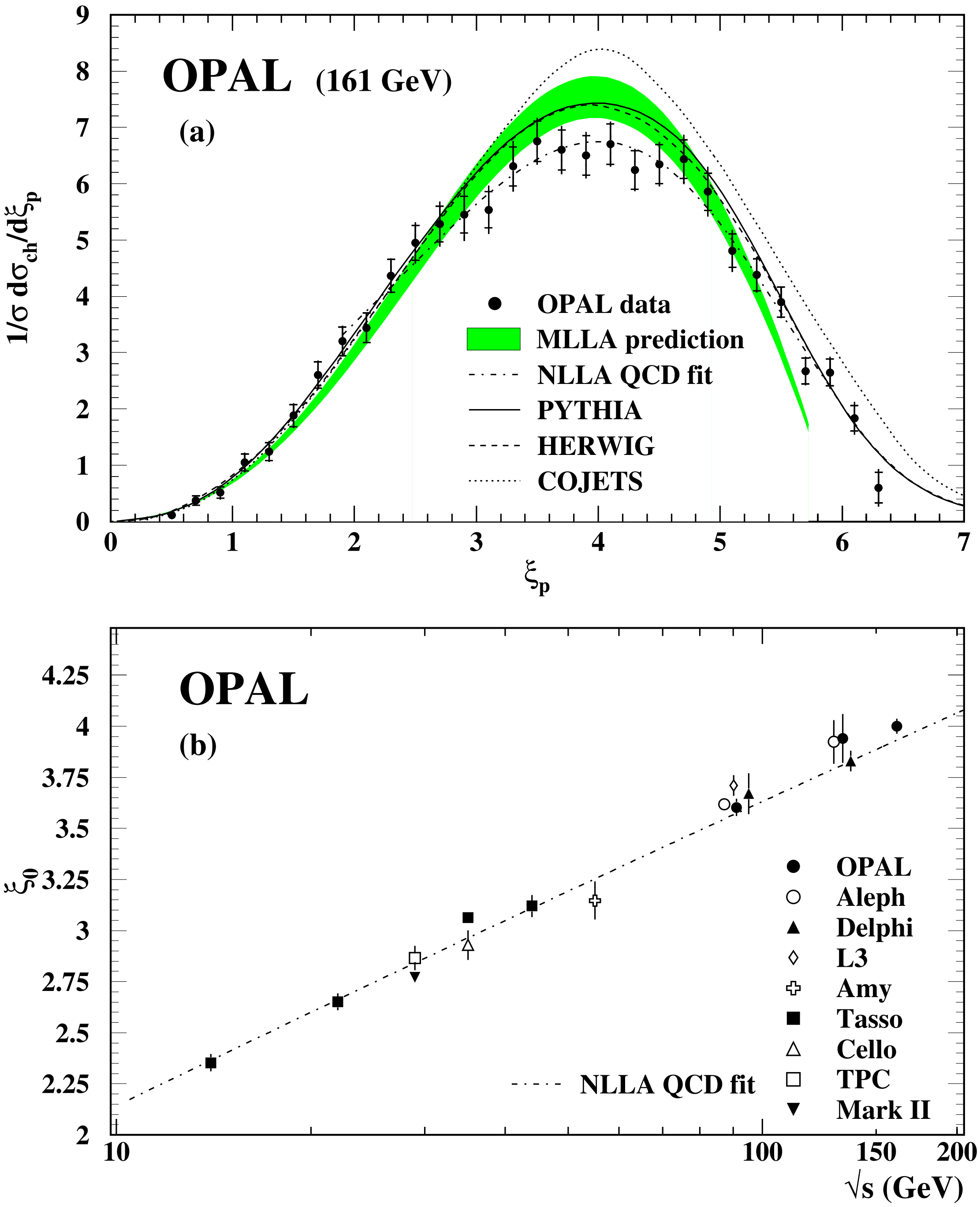

Figure 12: (a) Distribution of $\xi_p = \ln(1/x_p)$ for charged particles. Also shown are a fit of a NLLA QCD prediction, and predictions by MLLA QCD and PYTHIA, HERWIG and COJETS. The curve for the ARIADNE prediction is almost indistinguishable from the PYTHIA prediction and is omitted. (b) Evolution of the position of the peak of the ξ_p distribution, ξ_0, with c.m. energy $\sqrt{s}$, compared with a fit of a NLLA QCD prediction up to and including the data points at 133 GeV.

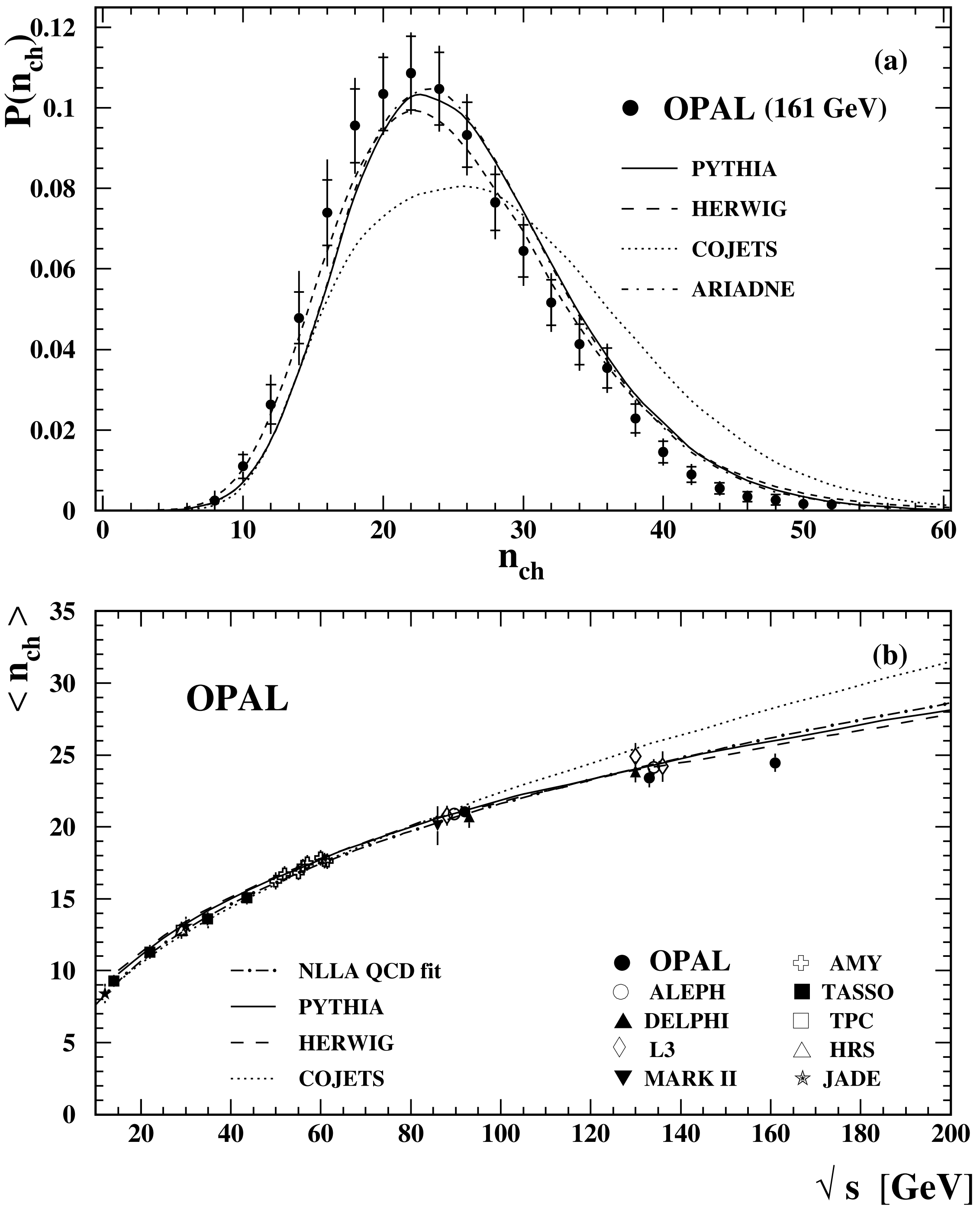

Figure 13: (a) Corrected distribution of the charged particle multiplicity n_{ch}. Predictions from PYTHIA, HERWIG, COJETS and ARIADNE are also shown. (b) Mean charged particle multiplicity measurements over a range of $\sqrt{s}$ from 12 GeV to 161 GeV. The measurements are compared to a fit of the NLLA QCD prediction for the evolution of charged particle multiplicity with $\sqrt{s}$ and to the predictions from PYTHIA, HERWIG, and COJETS. The curve for the ARIADNE prediction is almost indistinguishable from the PYTHIA prediction and is omitted.